Rock Mechanics and Rock Engineering
https://doi.org/10.1007/s00603-021-02406-1

ORIGINAL PAPER

Shear Response of Wet Weak Carbonate Rock/Grout Interfaces Under Cyclic Loading

Eleni Stavropoulou[1,2] · **Christophe Dano**[2] · **Marc Boulon**[2]

Received: 15 May 2020 / Accepted: 10 February 2021

Abstract
The development and construction of offshore wind farms requires the correct estimation of the friction that can be mobilised at the rock/grout interface. In conventional studies, the shear behaviour of a joint is usually investigated with laboratory tests under constant normal load/stress (CNL), however, in engineering practice, direct shear testing under constant normal stiffness (CNS) has been proved to be more realistic in the assessment of the development of the side shear resistance in rock grouted pile design. In this work, an extensive experimental campaign on the shear response of a weak carbonate rock (limestone) interface with grout is presented, in the frame of offshore wind turbines. First, basic mechanical testing is performed on the two interface materials in order to evaluate their mechanical properties. The output of these tests reveals not only the contrasting properties of the two interacting materials, but also the decreased response of the limestone in the presence of water. A series of monotonic shear tests (both under CNL and CNS conditions) on wet rough limestone/grout interfaces reveal the high impact of adhesion between the two materials to the mechanical response. Based on the monotonic results, a number of CNS shear tests under cyclic loading takes place, where different failure modes are observed dilatant and contractant response. The variability of the failure mode is strongly related not only to the adhesion created with the cast grout, but also to the limestone's micro-structural heterogeneity that manifests already after consolidation. The post-shear morphological state of the interface is analysed, while the variability of the failure surface and the presence of water gouge creation do not allow a clear correlation of the morphologfy to the mechanical response. Overall, the response of this type of weak rock interface where the properties of the grout are significantly higher, is governed by the behaviour of the rock.

Keywords Weak carbonate rock · Limestone–grout interface · Shear tests under constant normal stiffness · Cyclic shear loading · Monopiles · Wet conditions

1 Introduction

The design and construction of offshore wind turbines in weak to moderately strong carbonate rock formations in the north of France, is considered and studied since a few years. Monopiles of a diameter varying between 7 and 10 m, and a height between 10 and 20 m, or smaller piles supporting a jacket structure (typically of a diameter between 2 and 3 m), will be possibly drilled in a hosting rock mass (calcarenite, limestone) and once installed, they will be sealed with grout (Fig. 1). The frictional resistance of the piles derives from the weakest interface within the structure, them being principally two: the rock/grout and the steel/grout interfaces. The steel/grout shear strength is in principle enhanced by shear keys and while still under investigation (Schaumann et al. 2010; Lotsberg et al. 2013), it is generally assumed to be higher than this of rock/grout that eventually controls the axial shaft resistance. The contrasting properties of the hosting rock mass and the filling grout make the study of the shear response of this interface essential for the design of offshore wind turbine foundations.

The application of an axial load on the pile will result in an initially elastic vertical displacement without a necessary activation of the pile/rock interface in shear. However, an increased axial force will introduce additional vertical displacement on the pile, triggering relative movement between

✉ Eleni Stavropoulou
eleni.stavropoulou@epfl.ch

[1] Ecole Polytechnique Fédérale de Lausanne (EPFL), Laboratory for Soil Mechanics (LMS), EPFL-ENAC-LMS, Station 18, 1015 Lausanne, Switzerland

[2] CNRS, Grenoble INP, Institute of Engineering, Univ Grenoble Alpes, 38000 Grenoble, France

Published online: 15 March 2021

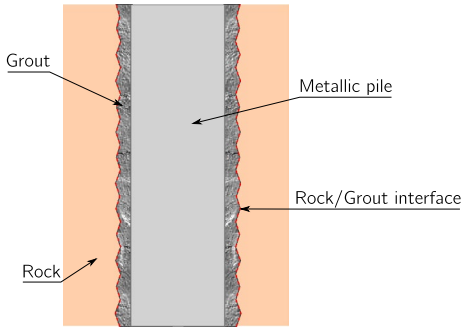

Fig. 1 Schematic illustration of the pile's installation and sealing in the rock formation

the pile and the rock mass. These additional vertical displacements can take place according to two principal mechanisms, depending on the characteristics of the grout, the pile and the rock mass, as well as the in situ stress conditions and the roughness of the interface (Johnston et al. 1987).

The first mechanism involves sliding of the rough pile shaft over the asperities on the socket wall (see Fig. 2b), causing the socket diameter to dilate against the radial stiffness of the rock mass. Consequently, the stresses acting normal to the pile shaft will increase as the dilation increases, leading to an increase in shear resistance. This dilatant sliding mechanism will continue until the resistance to further sliding exceeds the shear resistance through the effective asperity area. The second mechanism consists of the asperities of rock on the socket wall being sheared off with no dilation of the socket and thus, no increase in normal stress nor shear resistance (contractant response). In the case of weak rocks (chalk, weak limestone etc.) the dilatant mechanism is somewhat limited and a contractant response takes place rapidly.

For the dilatant sliding mechanism, the rate of increase in normal stress $\Delta\sigma_n$, with dilation Δr, is effectively constant and given by:

$$\frac{\Delta\sigma_n}{\Delta r} = \frac{E}{1+\nu} \times \frac{1}{r} = \frac{2G}{r} = k \tag{1}$$

where, E is the rock mass modulus, ν the Poisson's ratio of the rock, r the radius of the pile and k the medium's normal stiffness. It follows that the dilation of the socket results to an increase in the stress acting normal to the pile shaft and that relative movement between the pile, and the rock is controlled by constant normal stiffness (CNS) (Johnston et al. 1987; Indraratna et al. 2005) as opposed to the more conventionally encountered conditions of constant normal load or stress (CNL) (Ladanyi and Archambault 1969; Tatone and Grasselli 2015).

The importance of borehole roughness to shaft resistance has been well recognised and quantified. While (Seidel and Haberfield 1995) recommended that roughness is scale dependent and its evaluation is accompanied by a meaningful measure of scale, Nam and Vipulanandan (2008) investigated the effect of drilling tools on socket roughness on drilled shafts socketed in limestone and clay-shales. Seidel and Haberfield (2002) suggested the use of the "Monash socket roughness model" to analyse statistics of socket roughness. This method is based on an idealised joint interface as a series of interconnected chords with a constant length, l_a, as shown in Fig. 3a. It is assumed that

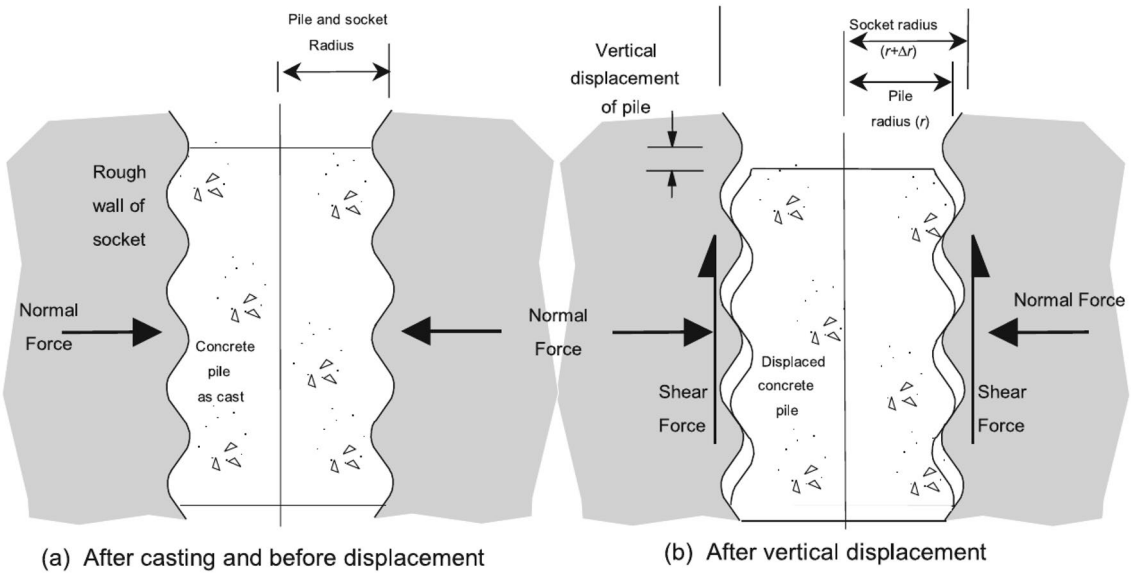

Fig. 2 Idealised displacement of pile socketed in rock (Johnston et al. 1987)

the chord angles $\theta°$ follow a Gaussian distribution, thus the asperity heights Δr can be expressed as the average height of all asperities (Fig. 3b).

Nam (2004) suggested that roughness can be represented by a regular saw-tooth with a chord length l_a and roughness height Δr corresponding to a roughness angle $\theta°$ adopted on the basis of the used drilling tool. As such, for a given drilling tool (and rock type), the corresponding roughness angle is chosen. Based on the scale of the rock sample, values of l_a and Δr are varied to fit the chosen angle $\theta°$. Seidel and Haberfield (2002) discussed the importance of realistic roughness modelling for representative laboratory testing, by comparing the response of interfaces with regular triangular asperities to the response of irregular profiles produced based on the fractal model of Seidel and Haberfield (1995). Their experimental results on unbonded rock/concrete interfaces show a more brittle response of higher shear resistance for regular triangular asperities, compared to a ductile response of lower peak shear stress for the corresponding irregular profile. Such results reveal the necessity of representative profiles for an accurate evaluation of large scale problems. Nevertheless, the study of regular triangular interfaces is a useful step in understanding the performance of the more complex natural interfaces.

In this paper, the shear behaviour of a bonded rough (regular triangular asperities) limestone/grout interface is studied with lab-scale shear tests under constant normal stiffness (CNS) in wet conditions (offshore applications). A first part is dedicated to the study of the mechanical properties of the two composing the interface. Afterwards, the shear response of the interface is investigated with a series of monotonic tests under different levels of applied normal load and stiffness. The results of the monotonic tests are taken into account for the design of the following experimental campaign on the shear characterisation of the interface under cyclic loading. The failure mechanisms are explored taking into account the contrasting mechanical properties of the two materials composing the interface, as well as the post-shear geometrical profile of the samples.

2 Materials Characterisation

The lack of previous database on the geomaterials constituting the studied interface motivated a short study on their basic mechanical properties that is presented in this section. The evaluation of these properties is of great importance for the interpretation of the mechanical response of the interface.

2.1 Saint Maximin Limestone

Carbonate rocks present high micro-structural heterogeneity, which can be even more significant based on the site location. In this study, a Saint-Maximin limestone is used. The Saint-Maximin limestones come from a quarry to the north of Paris (Saint-Maximin, France) and seem macroscopically homogeneous. These rocks which were formed 45 million years ago, are beige coloured sedimentary limestones composed of calcite and quartz. A sediment bedding commercially denoted "Roche Franche Fine" (RFF) is selected. The RFF limestone has fine solid phases, in which large fossils can be found. Their porosities determined by hydrostatic weighing vary between 25 and 35% (Rozenbaum and du Roscoat 2014).

A dry cylindrical rock sample ($d = 40$ mm, $h = 80$ mm) has been scanned with X-ray tomography in the 3SR Lab in Grenoble. A vertical slice of the 3D X-ray image (55 μm/px), as well as three horizontal slices at different heights in the sample are presented in Fig. 4. One can immediately notice the great heterogeneity that this carbonate rock presents in its structure—at least at the observed (meso-)scale. When looking at the vertical slice, two distinct layers can be easily observed, above and under the BB line, where the porosity varies in a significant way. The three horizontal slices let some more insight to the heterogeneous structure of the rock sample. A clear transition from a high to a much lower porosity is observed from slice A to C, with very large pores at times (low density, black colour) or big inclusions (high density, white colour) and shells (slice C).

This heterogeneity is not visible to the naked eye and can be responsible for potential variability in the mechanical results of similar in size samples. Even though some

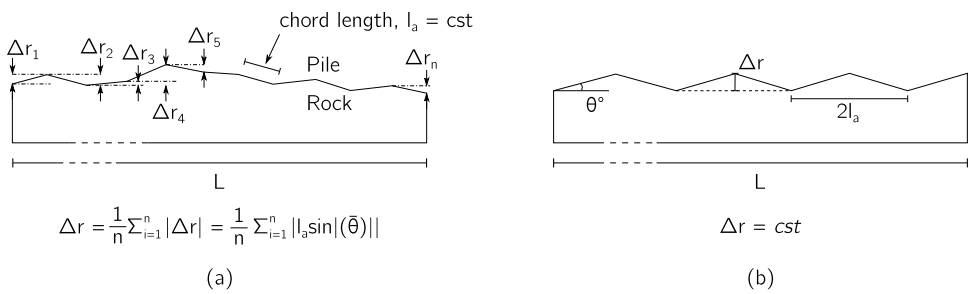

Fig. 3 **a** Monash Socket roughness model (Seidel and Haberfield 1995), **b** idealised saw-tooth surface (Nam 2004)

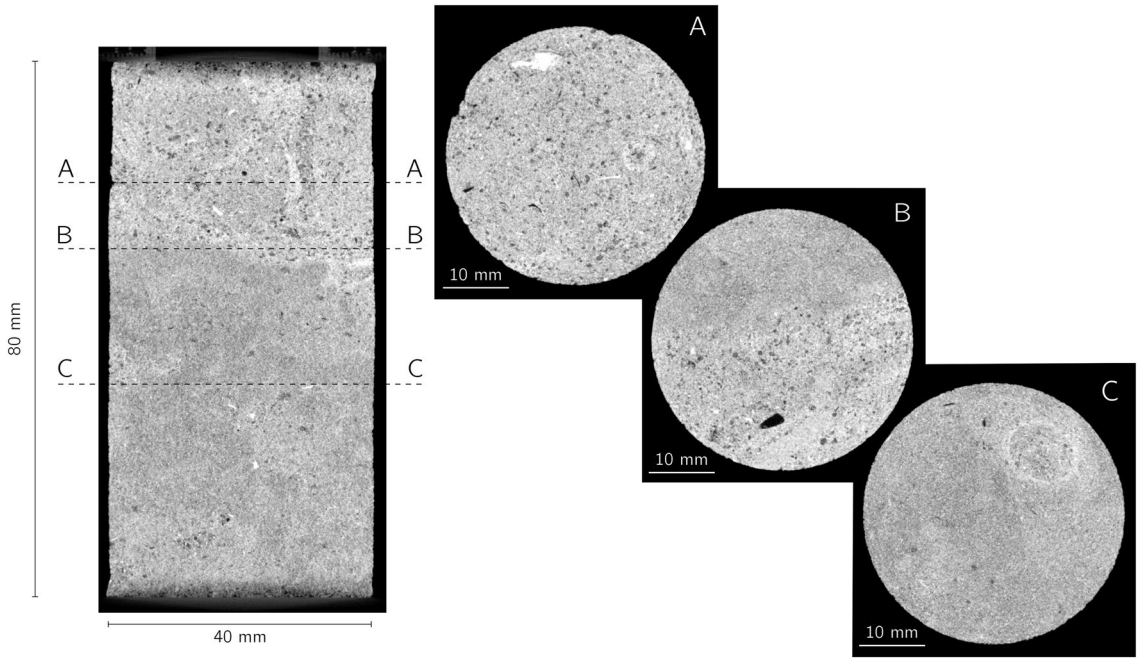

Fig. 4 X-ray tomography images of a limestone sample; left: vertical slice, right: horizontal slices at different heights, *A*, *B* and *C*

Table 1 Global results of the mineralogical analysis, + + +: predominant/very abundant; ++: abundant; +: scarce; Tr: traces

Calcite ($CaCO_3$)	Quartz (SiO_2)	Aragonite ($CaCO_3$)	Phyllosilicates	Ankerite $Ca(Fe,Mg)(CO_3)_2$	Anhydrite ($CaSO_4$)
+ + +	+	+	+	Tr	Tr

Table 2 Tensile (σ_t) and unconfined compressive strength (σ_n) of the Saint Maximin RFF limestone

		Mean	Min	Max
σ_t (MPa)	Dry	1.53	1.30	1.64
	Wet	0.88	0.82	1.97
σ_n (MPa)	Dry	8.15	7.95	8.35
	Wet	6.19	6.01	6.32

interesting qualitative observations on the material's structure can be made, a more quantitative analysis in this resolution is challenging due to the existing heterogeneity. Here, heterogeneity does not only refer to the geometry of the solid skeleton, but most importantly to the mineralogical composition of the material that does not allow an accurate contrast between the solid phase and the pores.

In addition to the structural observations from X-ray images, a mineralogical analysis using X-ray diffraction has been performed, the results of which can be found in Table 1. The obtained results confirm the dominant presence of calcite, as well as the existence of quartz and other carbonate based minerals.

The basic mechanical properties of the Saint Maximin limestone are investigated with a series of brazilian (tested samples: $d = 40$ mm, $h = 20$ mm) and simple compression tests (tested samples: $d = 40$ mm, $h = 80$ mm). Both dry and wet samples have been tested in order to evaluate the impact of water presence to the response of the material.

Dry conditions are achieved in a furnace at 80 °C, while wet conditions are applied by soaking the samples in free water until mass stabilisation. The term wet is preferred to saturated, as total saturation is not accurately measured.

Table 2 presents the measured tensile (ASTM D3967-16) and unconfined compressive (ASTM D2166-00) strength of the material for both dry and wet conditions. A significantly lower response is encountered in the presence of water both in tension (wet 43% lower than dry) and compression (wet 27% lower than dry). These results point out the significance of the hydric state of the limestone to its mechanical response that have to be taken into when investigating offshore conditions. A possible explanation of this response could be related to the chemical interactions that occur to the limestone structure in the presence of water and lead to weakening of the rock matrix and therefore, earlier and faster failure (Lebedev et al. 2014). Chemical reactions between fluid and rock material may result in partial dissolution of the rock's carbonate minerals (here, calcite), increase of porosity and eventually reduced strength (Rhett and Lord 2001; Vanorio and Mavko 2011). Several laboratory studies have shown that the shear modulus can be

reduced when the rock changes from dry to saturated conditions (Assefa et al. 2003; Røgen et al. 2005). The main factors inferred to be responsible for that reduction are carbonate pore types (Baechle et al. 2005) and pore connectivity (Rossebø et al. 2005; Misaghi et al. 2010).

Finally, the elastic properties of the limestone are measured with simple compression tests, with the aid of two strain gauges perpendicular to each other. Unlike the response at failure, the elastic response is measured rather similar for the dry and wet conditions as shown in Table 3, supporting the idea that water affects crack propagation after initial elasticity (Alonso et al. 2012).

2.2 Grout

For the creation of the interface, a cement grout is used i.e. water and cement only, according to the following recommendations: $w/c < 0.45$ and $c \leq 600$ kg/m^3 (recommendations DNV OS-C502 AS 2013). The testing formulation is chosen to: $w/c = 0.40$ and $c = 694.5$ kg/m^3.

Cylindrical samples ($d = 50$ mm, $h = 100$ mm) are tested in unconfined compression at different ages; 7, 28 and 90 days. All samples have been cured in water after casting (i.e. after 24 h), they are therefore considered fully saturated. The results of the unconfined compression tests are shown in Fig. 5. Already after 7 days, the grout sample reaches a compressive resistance of around 40 MPa, i.e. 5 and 6.5 times higher than the one of the dry and wet limestone respectively. The compressive strength does not vary significantly at older age, and thus, an average compressive resistance of 42.5 MPa is considered for the given grout formulation. Unlike the compressive strength which does not significantly vary with age, the measured stiffness of the grout samples increases with age (Table 4).

3 Characterisation of the Rock/Grout Interface in Shear

The study of the two geomaterials in the previous section revealed the significantly lower strength of limestone compared to grout. Taking this into account, failure is most likely to occur in the limestone part of the rock/grout interface. In this context, an accurate study of the interface requires a preliminary characterisation of the rock's resistance in shear, which will then be compared to the response of the rock/grout interface. In this section, the interface sample preparation is presented, followed by the experimental campaign on the characterisation of the rock/grout interface under monotonic loading, with a series of CNL and CNS shear tests.

3.1 Samples Preparation and Experimental Device

A metallic square shear box composed by two half shear boxes is used as mould for the preparation of the interface samples. Based on the sample configuration presented in Fig. 6a, the rock sample ($L \times W = 100$ mm $\times$ 100 mm, $H =$ 50 mm) is placed in the bottom half shear box and positioned using an adjusting table in a way so that its mean surface is horizontal and 5 mm higher than the box. The prominent surface of the rock is laterally sealed by a plexiglas plate of 10 mm thickness, on top of which the second half shear box is centred and fixed by two screws. The grout is poured on top of the rock's surface, filling up the top half box. Once the grout hardens (usually the day after), the entire shear box is turned upside-down, exposing the unsealed rock. At this point, the top half shear box is detached and a round membrane is passed around the interface zone, which will later be used as a water reservoir. The half shear box is fixed back in place and the rock is sealed with the same grout.

Accordingly, a day later that the rock's sealing hardens, the plexiglas plate is removed and the round membrane is filled up with water in order to introduce and maintain the wet conditions of the interface sample. The removal of the plexiglas plate leaves a free rock/grout interface of 10 mm height and a 10 mm $\times$ 10 mm surface, with the joint being

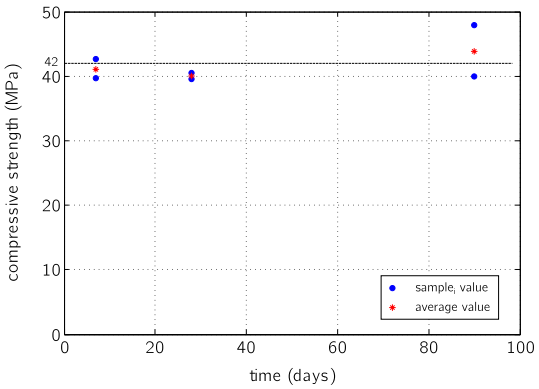

Fig. 5 Uniaxial compressive strength of grout samples at different ages (7, 28 and 90 days)

Table 3 Elastic properties of the Saint Maximin RFF limestone

Poisson's ratio, ν	0.13
Young's modulus, E (GPa)	5.6
Shear modulus, G (GPa)	2.16

Table 4 Deformation modulus of grout

Age (days)	E (GPa)
7	7.4
28	11.8
90	12.5

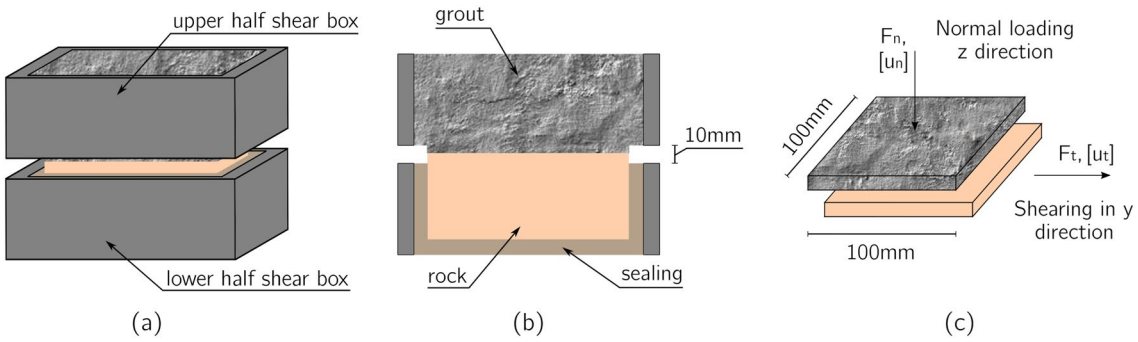

Fig. 6 **a** 3D illustration of an interface sample, **b** vertical cut of the interface sample, **c** illustration of the free interface and the measured parameters during a shear test

in the middle (Fig. 6b, c). The two screws hold the two half shear boxes together reassuring no relative movement of the interface during installation of the sample. Figure 7 presents in detail the exact preparation of a rock/grout interface sample. In the case of a rock/rock interface, the procedure is similar, except for step 5 (Fig. 75), where instead of grout, another rock sample of the same dimensions is placed and sealed on top of the exposed surface. The interface sample is left to cure for 14 days before tested.

As explained in the introduction, the roughness introduced by the drilling tool can affect the shaft resistance. Nam and Vipulanandan (2008) suggested that roughness can be represented by a regular saw-tooth with a chord length l_a and an asperity height Δr corresponding to a roughness angle $\theta°$ according to the used drilling tool. Based on these observations, triangular asperities of roughness angle $\theta = 5.7°$ are chosen for the rock specimens, corresponding to an asperity height $\Delta r = 0.5$ mm and a segment length $2l_a = 10$ mm (see Fig. 8a). Figure 8b shows a real rock sample of this specific roughness that has been created with a milling cutter for non metallic materials in dry conditions. In the case of a rock/rock rough interface sample, the two rock specimens are placed on top of each other, in a way so that the asperities are complementary and there is a perfect interlocking between

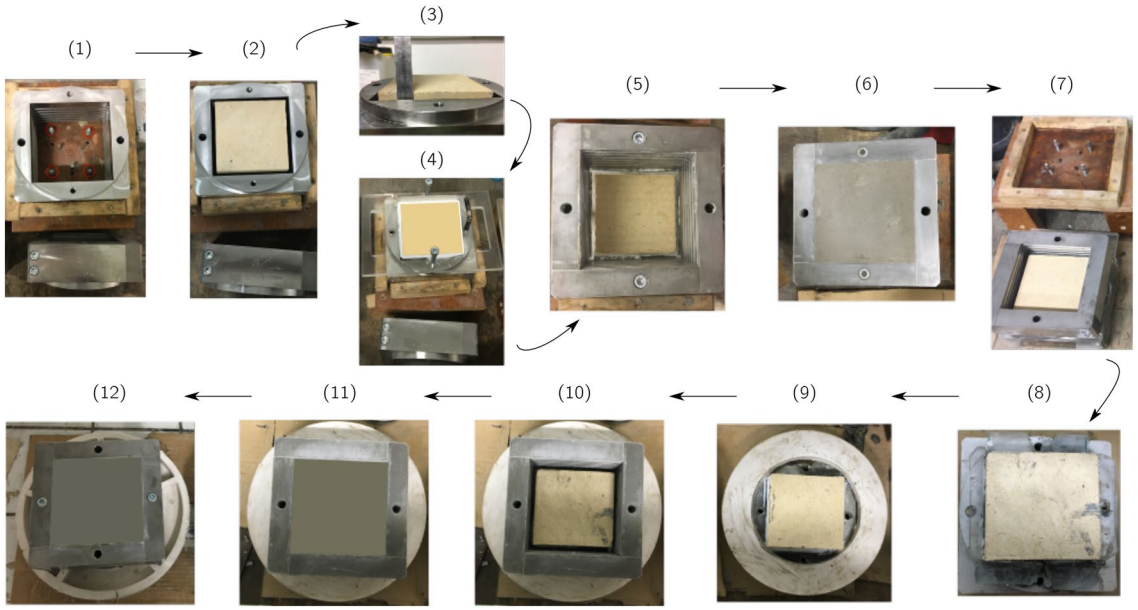

Fig. 7 Interface sample preparation: (1) and (2) positioning of the rock sample in the bottom half shear box with the aid of a table and four adjusting screws, (3) orienting the top surface horizontally, 5 mm above the bottom half shear box, (4) lateral sealing of the free surface with two plexiglas plates, (5) attachment of the top half shear box, (6) filling-up the top half shear box with grout, (7) upside-down turn of the entire shear box, (8) removal of the (now) top half shear box, (9) positioning of a round membrane around the level of the created interface, (10) fixation of the half shear box, (11) sealing of the exposed rock sample with grout, (12) upside-down turn of the shear box system which is left to cure for 14 days filling-up with water the membrane reservoir

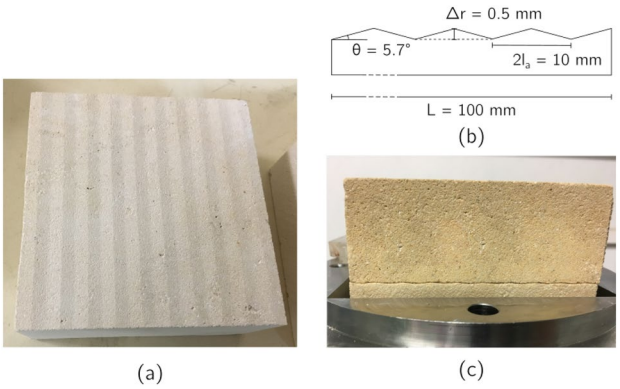

Fig. 8 Limestone sample with regular sawtooth roughness of constant asperity height and width

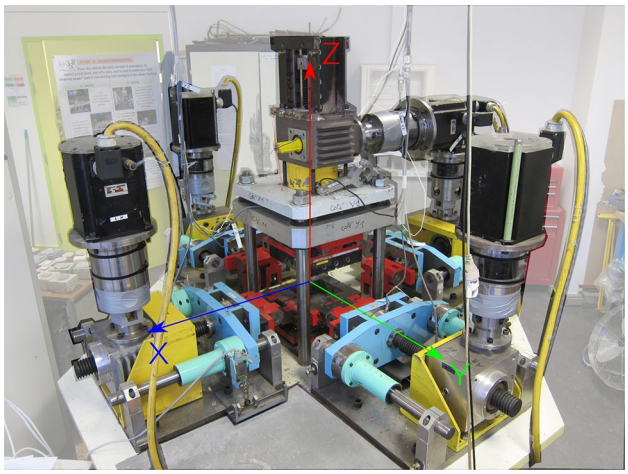

Fig. 9 The BCR-3D shear device with the three principal loading axes *X*, *Y* and *Z* (Stavropoulou et al. 2019)

them (see Fig. 8c). Evidently, in the case of a rock/grout interface, this interlocking is obtained naturally when casting the grout on top of the rough rock surface. Even though a fully bonded interface does not directly depict realistic field conditions, the contribution of the imposed adhesion to failure may introduce more complex mechanisms—other than sliding and asperities breakage—that could be attributed to the interface geometry based on the post-failure morphology. For this reason, the great majority of the studied rock/grout samples are fully bonded (directly cast grout), while the impact of the initial adhesion to the shear response is investigated with comparison to an unbonded rock/prefabricated grout interface.

3.2 Monotonic Shear Tests

In the following experimental campaign, the shear response under monotonic loading of two types of interfaces is studied; rock/rock interface and rock/grout interface. All shear tests are performed using the BCR3D shear box (Boulon 1995). This original shear device allows, unlike conventional shear boxes, the application of symmetrical displacement on both parts of the active joint, limiting any relative rotation between the walls of the interface. The BCR3D is composed by three orthogonal loading axes, each one independent of the others: a normal (*Z*) and two parallel (*X* and *Y*) to the interface plane axes, all three controlled either in force or displacement (Fig. 9). For this work only one horizontal axis is used (*X*). This experimental device can be used for all classical compression and shear test conditions: shearing under constant normal load (CNL), CNS or Constant Volume (CV).

In this work, all monotonic shear tests are controlled in displacement along the shear axis, while the normal axis is controlled either in stress (CNL) or stiffness (CNS) depending on the desired boundary conditions. An initial study with shear tests under CNL is performed, in order to determine the mechanical properties of the interface (friction angle and apparent cohesion). First, flat rock/rock interface samples are tested in shear, in order to define the residual response of the joint. Following, the contribution of roughness is studied with shear tests on regular sawtooth rough rock/rock interface samples. Finally, the mechanical properties of the rough rock/grout interface are investigated and compared to those of the rock/rock interface. The CNL tests are followed by two series of shear tests under CNS on rough rock/rock and rock/grout interfaces, these being the most representative to in situ conditions.

For each type of test (CNL or CNS) and interface (rock/rock or rock/grout) three different samples are tested. More precisely, in the case of CNL tests, a different normal stress is applied on each tested sample within the in situ range:σ_n = 100 kPa, 200 kPa & 300 kPa. For the CNS tests an initial normal stress σ_{n0} = 100 kPa is applied, followed by shearing under a different normal stiffness for each sample: k_n = 500 kPa/mm, 1500 kPa/mm & 2500 kPa/mm. This range of normal stiffness is considered for a maximum normal stiffness k_n = 3000 kPa/mm based on Eq. 1, for G = 2.16 GPa and D = 3 m (small jacketed monopiles). Shearing towards both directions (positive and negative) is applied on all interface samples, allowing the calculation and comparison of the mechanical properties on either of them.

It is important at this point to be reminded that all shear tests take place under wet conditions, with the aid of the round membrane reservoir. Table 5 sums up the different tests performed under monotonic loading.

Table 5 Summary of performed shear tests under monotonic loading

	Rock/rock	Rock/grout
CNL	3 (flat bonded) + 3 (rough bonded)	3 (rough bonded)
CNS	3 (rough bonded)	3 (rough bonded) + 1 (rough unbonded)

3.2.1 Constant Normal Load Tests

Each sample tested under CNL is subjected to one cycle of shear ($0 \rightarrow +u_t \rightarrow -u_t \rightarrow 0$) under a monotonic shear displacement rate of 0.01 mm/s. According to Seidel and Haberfield (2002), this rate is considered slow enough to allow full dissipation of excess pore water pressures in the rock during testing. The applied shear displacement is chosen equal to 80% of the asperities' width (i.e., $0.8 \cdot 2l_a = 8$ mm) in order to ensure achievement of the peak shear stress that is expected for a horizontal displacement that corresponds to the asperities' peak height (i.e. $l_a = 5$ mm). Figs. 10, 11 and 12 show the evolution of shear with normal stress for the different tested interfaces under Constant Normal Load. The Mohr Coulomb failure envelope is plotted for each shearing direction and the calculated values of friction angle and apparent cohesion for each shearing direction are presented within each figure. Finally, the post failure interface of a tested sample is also included in each figure for further evaluation of the results.

A friction angle $\phi^+ = 30°$ is calculated for the flat rock/rock interface (Fig. 10), while a low but not negligible apparent cohesion of 37 kPa is calculated most likely due to the water presence and a non-perfectly flat surface (micro-roughness). Shearing towards the opposite direction results in a slightly lower friction angle ($\phi^- = 26°$) and a slightly higher apparent cohesion (58 kPa—the meaning of which is only mathematical at this stage). The variation of friction angle and the level of apparent cohesion on a flat surface is expected to be very low, however, the presence of water encourages the creation of a gouge which can affect these results.

As shown in Fig. 11, the introduction of asperities leads to an increase of friction angle to $\phi^+ = 38°$ and a higher apparent cohesion of 62 kPa. The increase of friction angle is similar (slightly higher) to the initial asperities angle ($\theta = \imath = 5.7°$, where $\imath$ is the dilation angle) (Patton 1966). When shearing towards the opposite direction, the friction angle is calculated equal to the friction angle of the flat interface, revealing the elimination of the initial asperities. This can be confirmed when looking at the post-shear state of the interface sample, where creation of gouge and total breakdown of the asperities are encountered.

Finally, the evolution of shear with normal stress of the three bonded rough rock/grout interfaces is presented in Fig. 12. A Mohr Coulomb failure envelope is plotted for the maximum shear strength at the initial application of shear displacement continuous line, which soon after drops in a considerable way (residual, dashed line). More precisely, the friction angle at the beginning of the shear application is calculated $\phi^+ = 62°$ significantly higher than the rock/rock interface. After failure, the residual friction angle is found lower ($\phi^+ = 44°$), while when shearing towards the

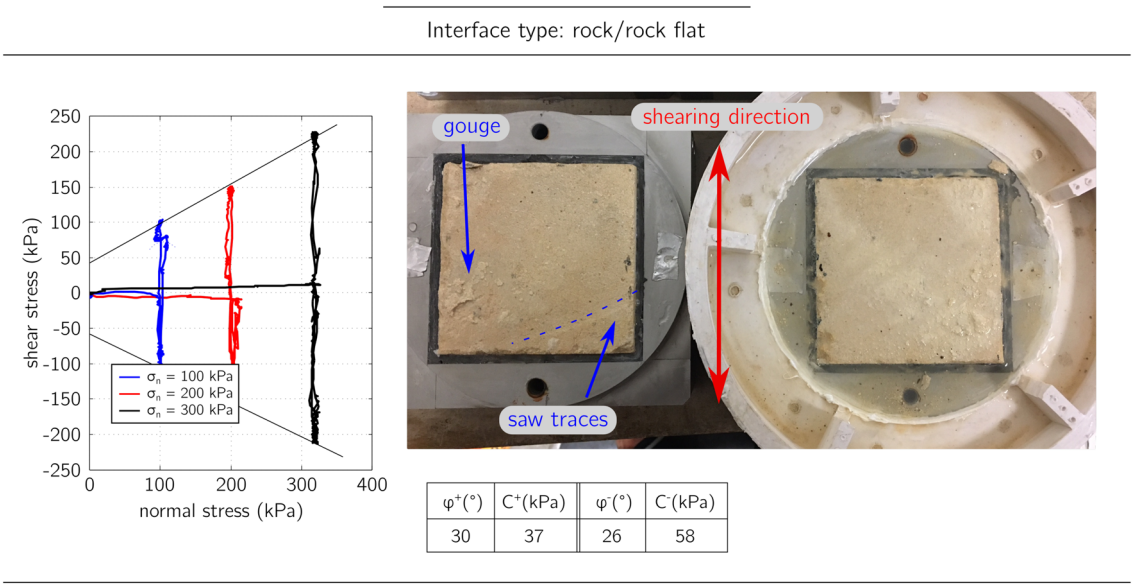

Fig. 10 Evolution of the normal with shear stress during the first cycle of shear under CNL for the three flat rock/rock tests—Mohr Coulomb failure envelope for the two shearing directions. On the right, the post-test surface state of the sample

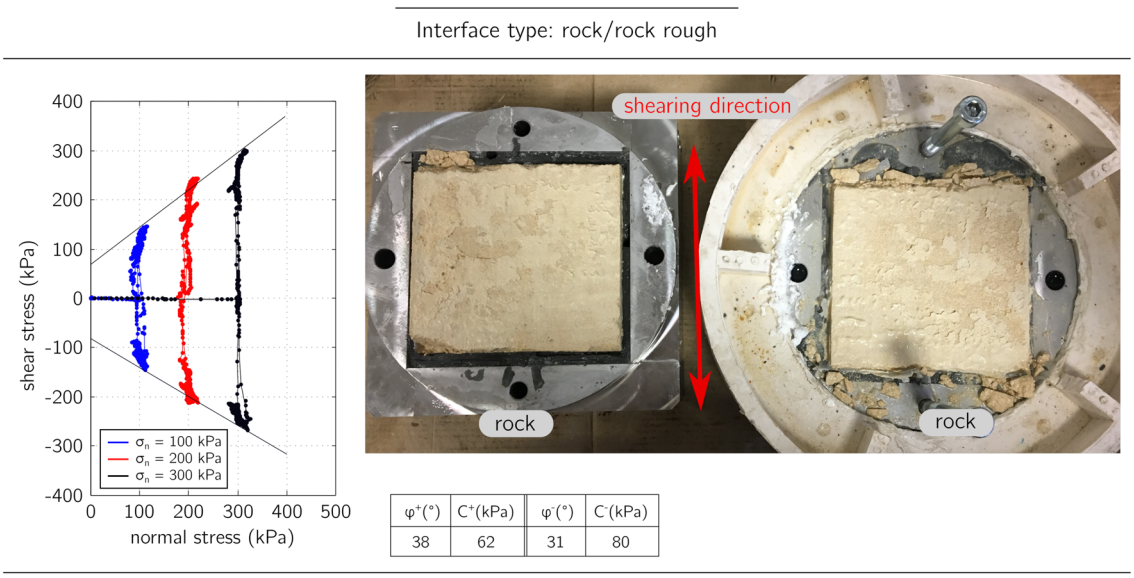

φ⁺(°)	C⁺(kPa)	φ⁻(°)	C⁻(kPa)
38	62	31	80

Fig. 11 Evolution of the normal stress with shear stress under CNL during the first cycle of shear for the three rough rock/rock tests—Mohr Coulomb failure envelope for the two shearing directions. On the right, the post-test surface state of the sample

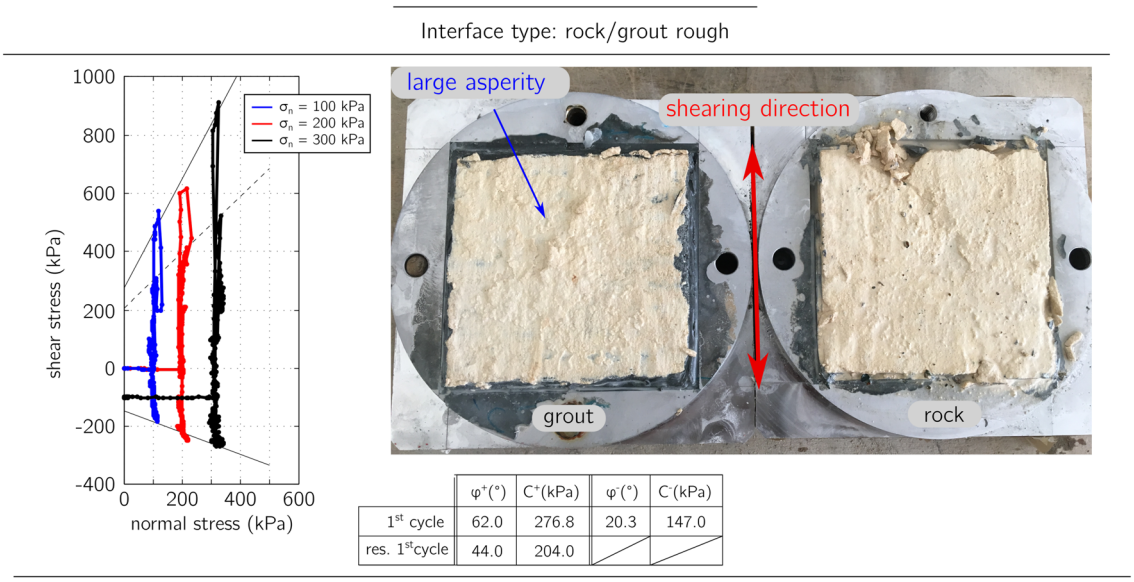

	φ⁺(°)	C⁺(kPa)	φ⁻(°)	C⁻(kPa)
1st cycle	62.0	276.8	20.3	147.0
res. 1st cycle	44.0	204.0		

Fig. 12 Evolution of the normal stress with shear stress during the first cycle of shear under CNL for all three rough rock/grout tests—Mohr Coulomb failure envelope for the two shearing directions. On the right, the post-test surface state of the sample

opposite direction the friction angle is calculated even lower ($\phi^+ = 20.3°$). The apparent cohesion during the first application of shear is, as expected, much higher than the rock/rock interface ($C^+ = 460$ kPa). This high value of cohesion can be physically explained by the pre-existing adhesion that was created during the casting and hardening of the grout on the limestone. After the first shear application the apparent cohesion also decreases when shearing towards the opposite direction.

In this type of interface, the two materials are strongly bonded (unlike the rock/rock interface), thus, the failure surface i.e. the shear surface after cohesion breakdown is not necessarily known a priori. The observation of the post-shear state of the rough rock/grout interface sample (Fig. 12) can give some more insight into the mode of failure. As one can immediately notice, a significant layer of rock has been attached on the grout, confirming that the failure occurs within the rock. The resulting failure surface can be irregular

as shown in the same figure, where a large asperity is created in the middle of the sample. Therefore, while one would expect a residual response similar to the rock/rock flat interface (Patton 1966; Johnston and Lam 1989), the irregularity of the failure surface can introduce significant variability in the results.

3.2.2 Constant Normal Stiffness Tests

A CNS shear test is controlled based on the following relation:

$$k = \frac{\sigma_n - \sigma_0}{u_n - u_0} \tag{2}$$

where, k is the applied normal stiffness (input parameter), σ_n is the current value of normal stress, σ_0 is the initial applied normal stress (input parameter), u_n is the current value of normal displacement, and u_0 is the normal displacement measured for σ_0 (input parameter) (Boulon et al. 1986). Based on the input parameters, the value of the measured normal stress is used in order to adjust the value of the current normal displacement to a constant stress/displacement ratio and therefore a constant normal stiffness throughout shearing.

For each shear test, an initial normal stress $\sigma_{n0} = 100$ kPa is applied and the corresponding normal displacement u_{n0} of the sample is noted. Even though the interfaces have been subjected to further shearing, the shearing path that has been considered for the calculation of the Mohr Coulomb failure envelopes is the following: $0 \rightarrow +85\%\ 2l_a \rightarrow +25\%\ 2l_a$.

Again, a shear displacement past the asperities' peak is considered for the evaluation of the shear resistance. The loading and shear rates are 10 kPa/sec and 0.01 mm/sec, respectively, for all performed tests.

Figure 13a presents the evolution of the shear with normal stress of the three rough rock/rock interface samples tested under different normal stiffness. A Mohr Coulomb failure envelope is plotted for each shearing direction. It is clear that the failure path is different compared to the CNL tests ($k_n = 0$) where the three shear stress peaks have been used for the calculation of the Mohr Coulomb envelope. In the case of a non-zero normal stiffness, the evolution of the shear stress follows the failure limit until total failure and thus, the Mohr Coulomb envelope is considered to pass from the peak value and following the evolution of the measured shear stress. The values of friction angle and apparent cohesion for each shearing direction are calculated and found similar to the calculated ones of the rough rock/rock CNL interfaces. This is expected, since friction angle is a property of the material, and the applied boundary conditions may only modify only the failure path. It is worthy to be mentioned that the term "material" is somewhat less absolute in the case of an interface that is de facto composed by more than one materials.

The last group of CNS tests is performed on bonded rough rock/grout interfaces. The evolution of shear stress with normal stress is plotted in Fig. 13b, together with the Mohr Coulomb failure envelopes for both shearing directions. The calculated values of friction angle and apparent cohesion are presented in the same figure. The friction angle is found similar to the one calculated for the flat CNL rock/

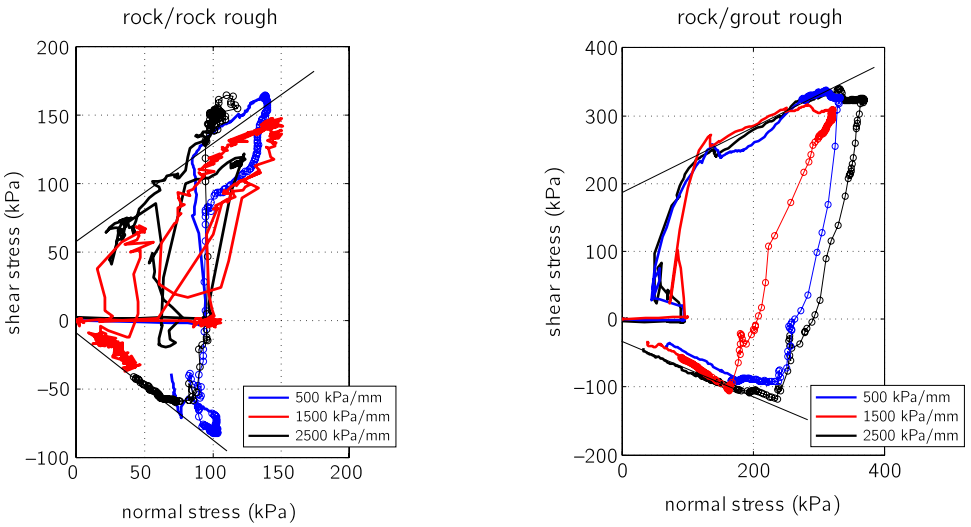

φ⁻(°)	C⁺(kPa)	φ⁻(°)	C⁻(kPa)
36.8	62.0	31.8	19.0

(a)

φ⁺(°)	C⁺(kPa)	φ⁻(°)	C⁻(kPa)
29.5	180.0	21.8	40.0

(b)

Fig. 13 Evolution of the normal stress with shear stress and Mohr Coulomb failure envelope for the two shearing directions **a** rough rock/rock interface, **b** rough rock/grout interface

rock interface, indicating once more failure within the rock. The apparent cohesion is again significantly higher than the rock/rock interface, but lower than the CNL test, since failure does not necessarily occur in the same way. This can be confirmed when looking at the post-shear state of the interface where the failure surface is rather variable.

The variability of the failure surface is mainly related to the bonding of the two materials. To verify the impact of bonding and therefore the origin of the observed variability, a rough unbonded rock/grout interface sample has been tested, using a prefabricated grout sample with complementary geometry to the in-contact rock. The prefabricated grout sample has been placed on top of the limestone sample, and the two parts were sealed in the two half shear boxes, leaving as usual a free rock/grout interface of 10 mm height. This interface is similarly tested in shear under CNS, under an initial normal stress $\sigma_{n0} = 100$ kPa and a normal stiffness $k_n = 1500$ kPa/mm. Figure 14 shows the results of the unbonded rock/grout interface. Similarly to the previous CNS tests, 3 cycles of shear have been applied, at the end of which shearing has been continued towards the negative direction up to a shear displacement $u_t = 0.85 \cdot 2l_a$.

The response of this type of interface follows with great accuracy the regular sawtooth geometry of the existing asperities. Peak shear stress is achieved during the first cycle at a shear displacement equal to the regular asperity length (see Fig. 14a at $u_t = l_a = 5$ mm), revealing a dilatant response until the asperities peak followed by a contractant response when continuing shearing downwards the asperities slope (Fig. 14b). A lower and less pronounced peak stress is measured during the two following cycles, again for a shear displacement equal to the asperities length, i.e. 5 mm. The decrease of shear stress with the cycles can be attributed to a progressive asperities breakage (in the limestone) that can be eventually verified from the decrease of the maximum normal displacement at each cycle in Fig. 14a.

The evolution of shear with normal stress is plotted in (Fig. 14c, continuous envelope). In both shear directions, the evolution of shear with normal stress follows the MC envelope since the beginning, unlike the bonded rock/grout rough interface (Fig.13b). The shear stress evolution reveals the different failure mechanisms of the two types of interface. For the unbonded interface, sliding and progressive asperities breakage (on the limestone part) occur at the application of shear. On the other hand, the evolution of the shear with normal stress of the bonded interface follows an initial increase of the shear stress until breakdown of the initial adhesion, followed then by sliding of the created interface (where the MC envelope is considered). Consequently, the failure response of the unbonded interface is similar to the bonded limestone/grout response (dashed envelope) in terms of friction angle $\phi^+ \approx 30°$. However, the initial apparent cohesion is as expected significantly lower when the grout is prefabricated $C^+ = 75$ kPa and exists mainly due to

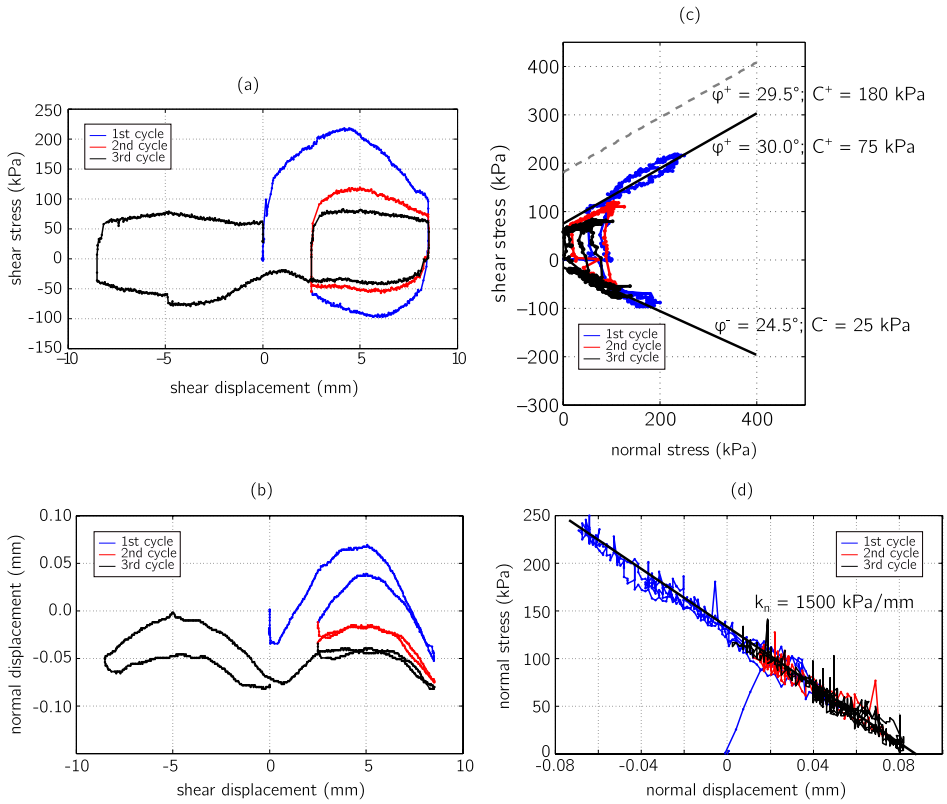

Fig. 14 Results of a prefabricated grout/limestone interface tested in shear under CNS

roughness. When shearing is applied towards the negative direction, both friction angle and apparent cohesion decrease as expected after some asperity damage.

Looking at the post-shear state of the prefabricated grout/limestone interface (Fig. 15), one can confirm that the failure surface occurs exactly at the interface between the two materials and the initial regular sawtooth roughness is preserved. These results point out the impact of pre-existing bonding to the mechanical response of the interface. For instance, the post-shear surface of bonded rock/grout samples is presented in Fig. 16. In all samples, failure occurs within the limestone resulting in a failure surface of a variable roughness. Even though a limestone layer is attached on the grout, the post-failure response of the bonded rock/grout interface can not be related to the rock/rock interface due to the post-failure roughness variability.

The overall results show a different failure mode of the rock/grout interface if grout is cast or prefabricated (bonded or unbonded, respectively). Field conditions involve casting of grout directly on the hosting rock, however, the interface may be smeared with cuttings that could prevent a perfect cementitious bond. This aspect needs to be considered before real site application since the fully-bonded laboratory conditions may overestimate the interface's response. The results of the monotonic shear campaign and the establishment of the Mohr Coulomb failure envelope for shearing under CNS isused for the design of the following part of this experimental campaign the study of the bonded rock/grout interface response under cyclic shear loading.

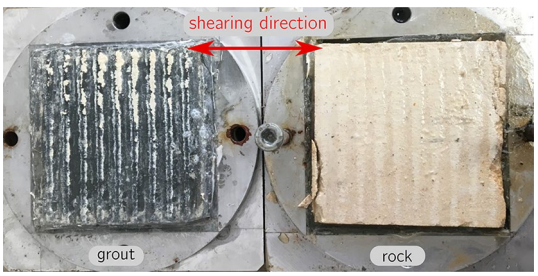

Fig. 15 Post-shear surface of the prefabricated grout and limestone rough interface (100 mm × 100 mm)

4 Investigation of the Rock/Grout Interface Response Under Cyclic Shear Loading

Cyclic loading is an important aspect of offshore design because the environmental loading during extreme weather conditions is generally more important than the permanent loading. In most cases the evaluation of the effect of cyclic loading relies on quantifying the reduction in shear strength (and hence foundation capacity) (Di Prisco and Muir Wood 2012; Liu et al. 2019).

Strain rates associated with cyclic loading are much higher than are typically used for monotonic laboratory tests. In most offshore design, the soil strength is adjusted globally by applying a reduction factor based on the severity of the cyclic loading. There are many idealisations that have to be made to achieve this, one of which is the representation of a storm loading sequence, with varying magnitude and period of the cyclic loading, by a uniform cyclic shear stress (Fig. 17I). Depending on the failure mode associated with the foundation, different stress paths will be followed in different parts of the failure mechanisms. The nature of the cyclic stress regime can be classified under four different types, ranging from symmetric two-way shear stresses to asymmetric two-way, ideal one-way and biased one-way (Fig. 17II). The last category, where the shear stresses do

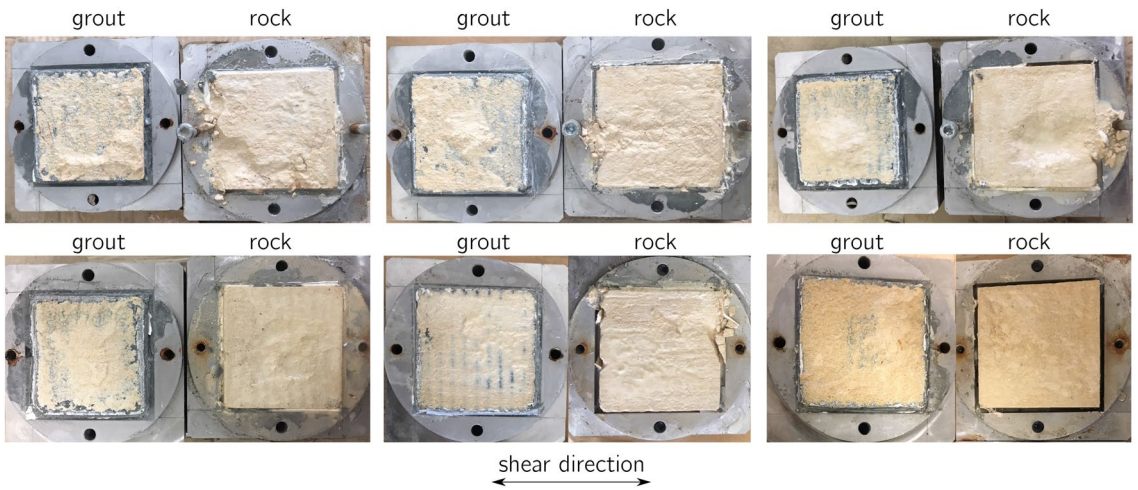

Fig. 16 Post-shear surfaces of bonded rough grout/limestone samples. In all cases, an irregular limestone layer is attached on the grout

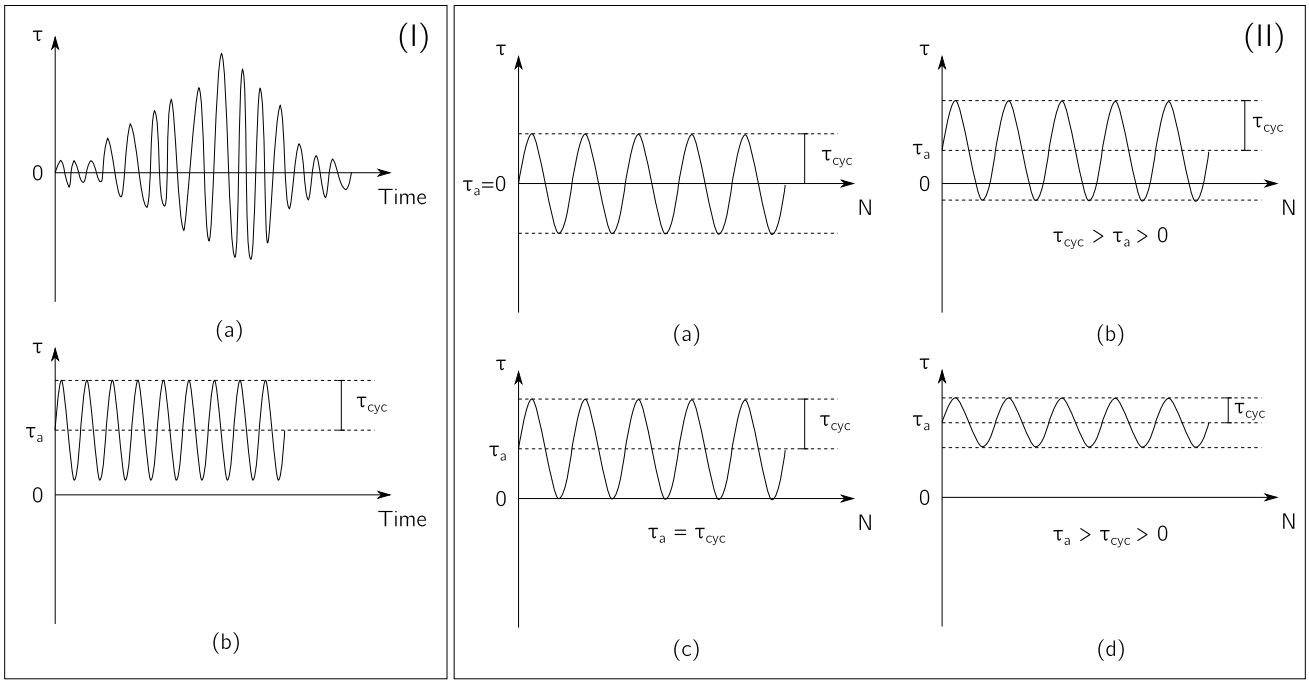

Fig. 17 (I) Contrast between field and laboratory cyclic shearing **a** cyclic forces from storm varying in amplitude and frequency, **b** constant stress amplitude and load frequency; (II) Classification of cyclic loading regimes according to the average τ_a and τ_{cyc} shear loading—2-way cyclic loading: **a** symmetric, **b** biased asymmetric and 1-way cyclic loading: **c** pure asymmetric, **d** biased asymmetric (Di Prisco and Muir Wood 2012)

not reverse in sign, is the least damaging type of cyclic axial loading, generally leading to mild accumulation of strains.

4.1 Experimental Campaign

A series of cyclic shear tests under CNS has been designed and performed on bonded rough limestone/grout interfaces. All interfaces present the same roughness with a regular asperity length and height as explained in Sect. 3.1 and are tested under wet conditions. Similarly to the monotonic tests, an initial normal stress $\sigma_{n0} = 100$ kPa is applied, followed by the application of cyclic shear loading under Constant Normal Stiffness. Figure 18 shows the performed shear tests that cover a wide range of one-way (seven tests) and two-way (seven tests) cycling loading. The different shear tests are described according to the applied shear load—average (τ_{ave}) and cyclic (τ_{cyc})—as a function of the shear strength ($\tau_{max,CNS}$) calculated from the monotonic shear tests and considered equal to $\tau_{max,CNS} = 310$ kPa (see Fig. 13b). The presented tests have been performed under an intermediate level of normal stiffness $k_n = 1500$ kPa/mm (in situ: $k_{n,max} = 3000$ kPa/mm). The notation of the different tests (for example "A1") is chosen based on the name of the used shear box (for example "A") and the block of limestone the rock part comes from (for example "1").

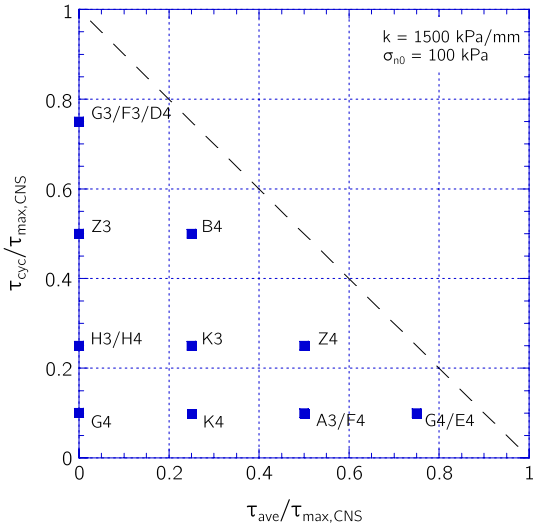

Fig. 18 Cyclic tests under constant normal stiffness

According to the monotonic results, the failure surface of a rock/grout interface can vary among the shear tests. This can result in a variable shear response among the tests which can for example be both dilatant or contractant even when repeating a shear test under the same loading. Taking into account this variable behaviour and knowing that failure

occurs within the limestone in a rather irregular geometrical/morphological way, the state of the interface has been studied in the early stage of consolidation—no application of shear yet—using X-ray tomography. More precisely, the 10 mm high free rock/grout interface is scanned before and after the application of a normal load $\sigma_{n0} = 100$ kPa to a stabilisation of the normal displacement.

Figure 19 shows the pre and post X-ray images of the interface in two different vertical slices of the 3D image. These images reveal that cracking occurs in the limestone already during consolidation, pre-determining a preferable failure geometry. The appearing cracks seem to be related to areas of variable density prior to consolidation, for example, where the contact between the two materials is not perfect (Slice 1) or where there are big pores in the limestone (Slice 2). The unbonded parts of the interface may also be related to the grout's shrinkage during its curing period, which could be favoured by the limestone's heterogeneous microstructure. The state of the limestone already after compression can explain the variability in the shear response: considering Slice 2, the first application of shear will result to a dilatant response if shearing is applied towards the right direction, whereas shearing towards the left direction will result to a contractant response.

Figure 20 shows the number of cycles to failure for each test performed under a constant normal stiffness $k_n = 1500$ kPa/mm. The samples that have been subjected to a shear loading close to the shear strength of the interface (τ_{cyc} and/or $\tau_{ave} \rightarrow \tau_{max,CNS}$) are expected to reach failure earlier, i.e. after a lower number of cycles. This is the overall tendency in the results presented in Fig. 20, which becomes even more coherent when separating the two types of cyclic loading: two-way and one-way. As expected, fewer cycles lead to failure in the two-way cyclic tests. The variability in the number of cycles to failure

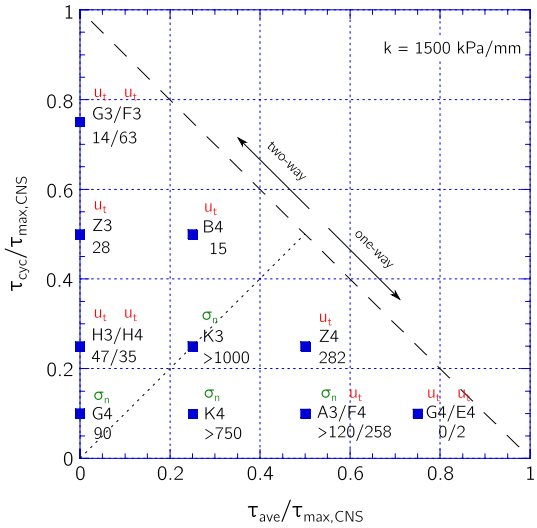

Fig. 20 Cyclic tests under constant normal stiffness with number of cycles to failure and modes of failure: σ_n for failure due to normal stress elimination and u_t for failure due to large increase of shear displacement

of the few tests that have been repeated can be explained by the variable and non-predictable state of the limestone after consolidation, that can favour the activation of different modes of failure with shearing. At the end of each cyclic test, a last monotonic shear application is performed in order to examine the post-failure response of the interface. The frequency of the performed cycles is constant and equal to $f = 0.005$ Hz (this frequency is related to the device's response capability to accurately follow the set value). While cyclic shear loading is controlled in shear force, the last shear application is controlled in displacement at a constant velocity of 0.01 mm/sec.

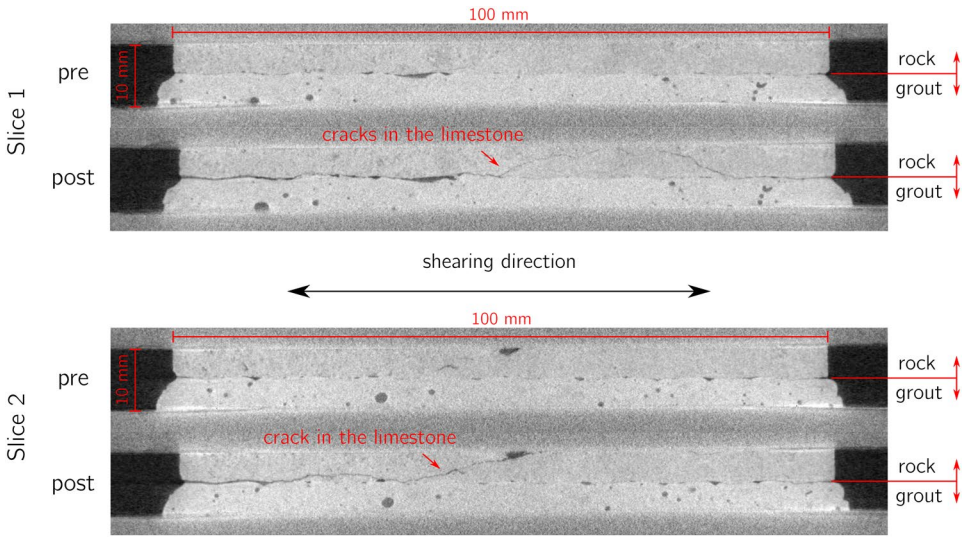

Fig. 19 Vertical slices of a rock/grout interface X-ray scan before and after application of normal loading

In the performed cyclic tests, two main failure modes have been generally observed: a large increase of the shear displacement as the sample tries to reach the applied shear stress or an elimination of the normal stress to zero, i.e. the interface is open and there is no active friction. In Fig. 20, the mode of failure is noted "σ_n" for failure due to normal stress elimination and "u_t" for failure due to increase of shear displacement. Almost all the samples tested in two-way cyclic loading have failed due to large shear displacement, while the one-way cyclic tests do not present a clear failure trend.

The results of two samples that present opposite failure response while tested under the same cyclic loading are presented and compared in more detail. Samples A3 and F4 have been tested in shear under a cyclic shear stress $\tau_{cyc} = 10\%\ \tau_{max,CNS} = 31$ kPa and an average shear stress $\tau_{ave} = 50\%\ \tau_{max,CNS} = 155$ kPa. The number of cycles to failure of sample F4 is almost twice the number of cycles of sample A3. In order to better evaluate the variable results, the evolution of the normal and shear stresses, as well as the normal and shear displacements of the two tests are plotted and discussed. In the following graphs each cycle is plotted in a different colour, while the average value of each parameter per cycle is plotted in black.

Figure 21 shows the evolution of the normal and shear stress, as well as the corresponding displacements per performed cycle for sample A3. The application of the shear stress is well maintained as shown in the first graph. In terms of shear displacement, a significant evolution is observed during the first 100 cycles which then stabilises. Along the normal axis, the stress decreases reaching to zero values approximately after 100 cycles, where failure is is identified (at 120 cycles). The decrease of normal stress together with the increase of the normal displacement reveal a contractant response of the interface. The stabilisation of the response during the following 600 cycles reveal that the interface is basically open and no further evolution is expected.

Subsequently, sample F4 is tested under the same loading and boundary conditions with sample A3. The evolution of the stress and displacement along the normal and shear axes for sample F4 is presented in Fig. 22. Once again, the applied shear stress is well maintained throughout the test in the desired range. The measured shear displacement is continuously evolving with the performed cycles, in a non constant rate, towards the opposite direction compared to sample A3, possibly indicating a different failure mode between the two samples. The different response between the two samples is more importantly depicted in terms of normal stress and displacement. The application of shear load leads to a jump in the normal direction which then continues increasing but in a less significant rate both in terms of measured stress and displacement. The test has been stopped due to the very high

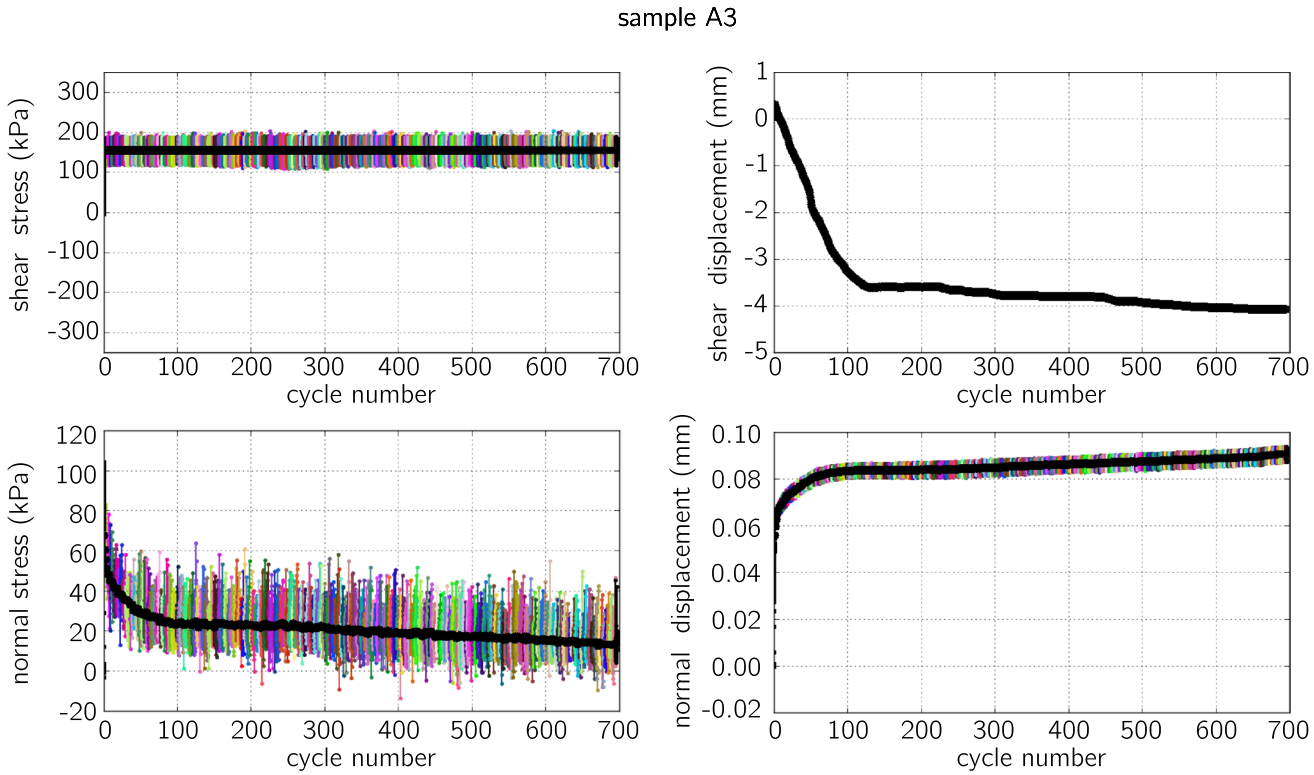

Fig. 21 Evolution of the measured parameters with the number of cycle (in black the average value per cycle)

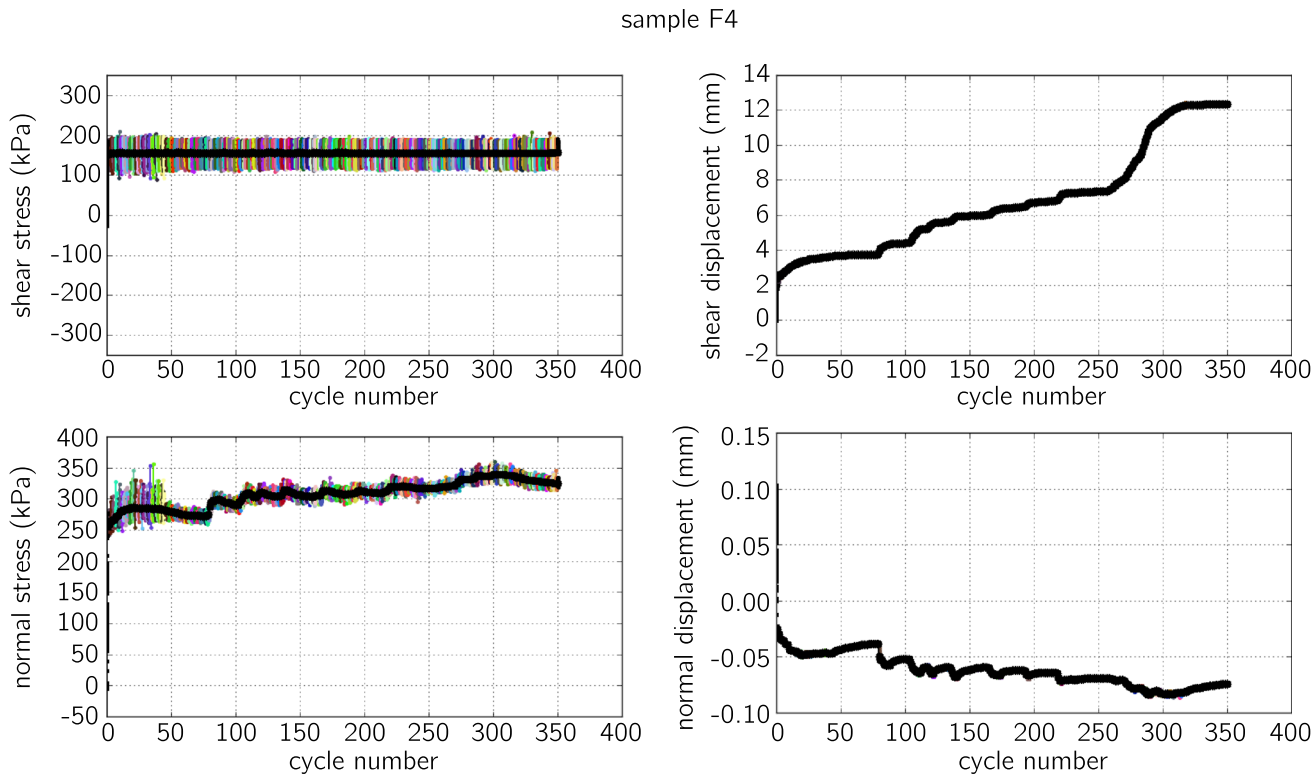

Fig. 22 Evolution of the measured parameters with the number of cycle (in black the average value per cycle)

shear displacement which reached the limits of one axis of the experimental device. The response of sample F4 is dilatant and could be explained based on the observation made in Fig. 19. Even though the two tested samples have been prepared and tested in an identical way, the microstructural heterogeneity of the limestone can lead to preferential cracking already since the application of the normal loading and therefore, affect the shear response based on the direction of the first application of shear.

A comparison between the two samples in terms of shear with normal stress can provide a better understanding of the two responses. Figure 23 shows the evolution of shear stress with normal stress of both samples A3 and F4; the response of the two samples in terms of normal stress is evolving in a completely different area in the stress plane. In the case of sample A3, the initial application of a normal stress σ_{n0} =100 kPa is followed by a decrease to almost zero with the application of the shearing cycles. On the contrary, for sample F4 the normal stress is jumping to a much higher value and continuously increases with cycles.

After these observations, it is interesting to evaluate the post-failure response of the two interfaces from cyclic loading. A large shear displacement is applied to each sample directly after the end of the cycles. The applied shear displacement is not pre-defined and it is continued up to a level where the shear resistance cannot be recovered. Indeed, the shear displacement cannot be related to the initial regular roughness of the interface, given its variable and unpredictable post-failure morphology (see Fig. 12). The evolution of shear and normal stresses is presented in Fig. 24. In the case of sample A3, further shearing leads to reactivation of the frictional surface with an increase of normal stress (σ_n =400 kPa) while maintaining the shear stress at $\tau \approx 270$ kPa. Final failure is reached with a very large shear displacement ($u_t \approx 23$ mm), after which the sample was unloaded.

Sample F4 has similarly been subjected to a last big shearing after the end of the cyclic loading. Shear resistance is maintained, however, for a very large shear displacement ($u_t \approx$=30 mm). Shear displacement towards the opposite direction has then been applied on this sample before final unloading.

Despite the opposite occurring mechanisms during cyclic loading, the post-cyclic failure response of the two samples is quite similar as highlighted with the encircled area on the two plots of Fig. 24. From the form of the evolution of the normal with shear stress of sample F4, it seems that the rock/grout interface tends to follow a residual response compared to the initially calculated monotonic Mohr Coulomb failure envelope (Fig. 13b). The peak point of sample A3 corresponds to similar values

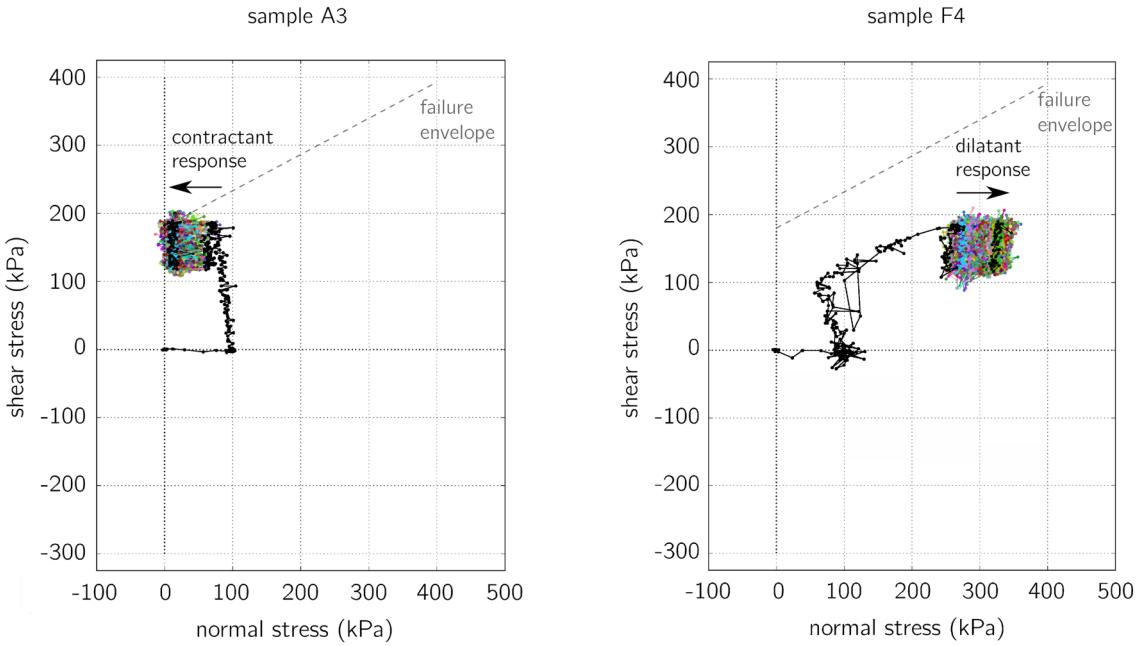

Fig. 23 Normal and shear stress during the performed cycles for samples A3 and F4

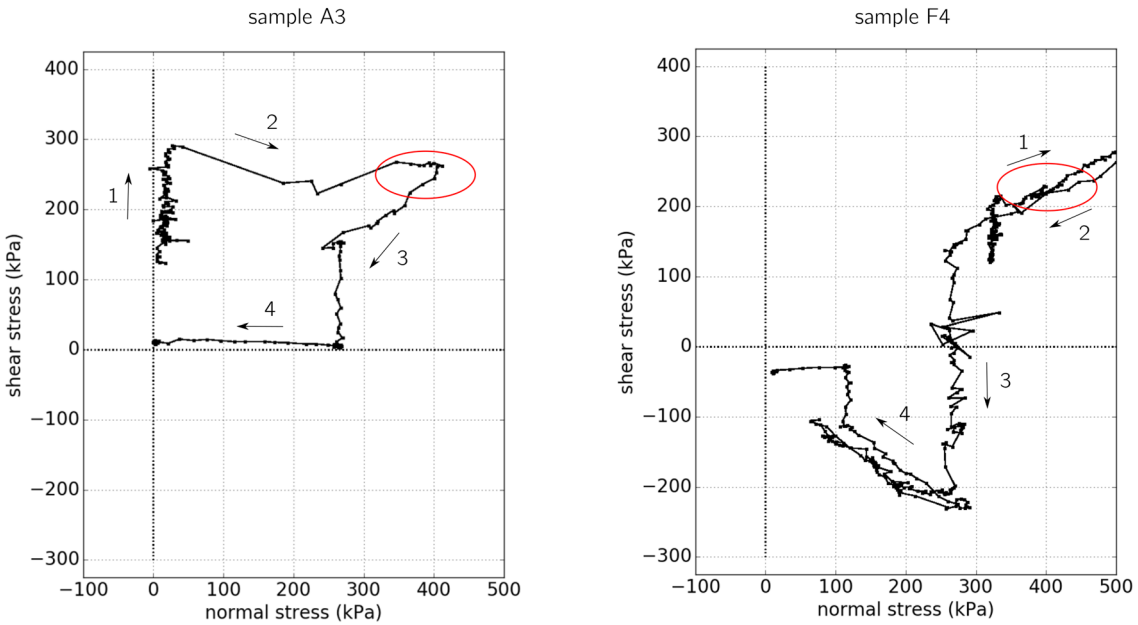

Fig. 24 Normal and shear stress during the application of a large post-cyclic failure shearing (the numbered arrows point the evolution of the curve during the test)

of normal and shear stress, revealing a similar residual response. From an engineering point of view, this is an important result which reveals that for either modes of failure the residual response of the interface at failure is the same.

5 Morphological Analysis of the Post-Failure Surfaces

It is well known that roughness is one of the main parameters influencing the shear response of an interface. In this work, all tested samples had the same initial roughness

(see Fig. 8). The experimental campaign presented above with shear tests on bonded rock/grout interfaces under either monotonic or cyclic loading, revealed a failure surface within the limestone. This failure surface is most of the times of an irregular roughness which is not easily predictable. However, the study of the post-shear morphology of the interface might be important for further interpretation of the mechanical results.

All tested interface samples have been scanned with a laser device. This scanning device moves horizontally in space (x, y) measuring the height (z) of each position throughout the scanned surface. The resolution along each horizontal axis is not the same; 0.05 mm along the x axis (shear direction) and 0.5 mm along y axis.

In the following paragraphs the topological maps of the post-shear scanned surfaces of samples A3 and F4 are presented, the mechanical results of which have been discussed above. The evolution, as well as the complementarity of the two post-shear surfaces are evaluated with the calculation of the average 2D profile along the shear direction (average of x profiles). To this average profile, a principal wave is fitted applying a Fourier transform and taking into account the lowest frequency, thus, the highest wavelength. The wavelength (λ) and amplitude (A) of the fitted principal wavelength is compared to the initial roughness ($\lambda = 10$ mm, $A = 0.5$ mm).

Figure 25 shows the two parts of sample A3 after the cyclic shear test. The two parts are quite complementary with a large part of the limestone on the upper corner being attached on the grout surface. The mechanisms behind this localised failure could be due to the heterogeneity of the limestone or the favourable failure conditions at the free boundaries. The fitted profiles are very similar for the two surfaces both in terms of wavelength and amplitude, which are very different from the initial existing roughness of the interface.

The two post-shear surfaces of sample F4 are scanned and their topological maps are plotted in Fig. 26. The different mechanisms of failure compared to sample A3 can be suspected in their morphological post-shear state. In the case of sample F4, a detached limestone asperity seems to have dominated the interaction between the two parts of the interface, leaving behind a trace all along the shear length. The traces of the initial roughness are obvious on the grout surface revealing that during this test, the actual shearing occurred principally between the predominant asperity attached on the grout and the equivalent zone on the limestone. The average 2D profiles of the two surfaces are plotted below together with the fitted ones. The two fits are similar for the rock and the grout, however the actual grout profile is composed by more distinguished asperities.

What is interesting in the post-shear state of most samples is that the initial interface roughness is still detectable on the grout surface but not on the limestone. This is revealed from both the topological maps and the average 2D profile plots. Consequently, even though failure occurs in the limestone there must be a considerable amount of gouge that is produced with shearing and is either evacuated during the test or redistributed, affecting partially the final morphological state of the two surfaces.

On the other hand, the traces of the initial sawtooth roughness can be detected on the grout surface, revealing the absence of a thick layer of attached limestone. This post-shear state can be explained by the creation and distribution of gouge or loss of limestone material when shearing in the presence of water. An important amount of created gouge can also be suspected in the cases where the two post-shear surfaces are not complementary. For example when a limestone part is detached but cannot be identified attached on the grout surface, it has most probably been lost or redistributed in the form of wet gouge on the two surfaces. Consequently the two surfaces do not present similar average profiles, but rather different values of wavelength and amplitude.

On the contrary, the post-shearing surface state of the unbonded prefabricated grout/limestone interface is very close to the initial one. As one can confirm from the topological maps and the average 2D profiles in Figs. 27 and 28, the initial roughness is overall very well preserved with only a decrease to half of, the asperities' fitted amplitude.

6 Conclusions and Perspectives

In this paper a detailed experimental program is presented, on the mechanical characterisation of the shear behaviour of a weak carbonate rock/grout interface in the context of offshore wind turbines design. An initial characterisation of the two materials consisting the interface "limestone and grout" has been necessary in order to correctly interpret the interface's response. First, the observation of the limestone's micro-structure with 3D X-ray scans a significant micro-structure heterogeneity with variable porosity. Then, the basic mechanical properties of the studied limestone are identified in both dry and wet conditionsrevealing a non-negligible impact of the water to the response; lower tensile and compressive strength in wet conditions. Finally, the compressive strength of the grout is measured more than 5 times higher than the limestone's (both dry or wet), revealing the striking contrast in the properties of the two materials composing the studied interface.

The limestone/limestone and limestone/grout interfaces are then tested in shear through a series of monotonic tests under two different boundary conditions: a first characterisation under constant normal load (CNL), followed by a characterisation under constant normal stiffness (CNS), the

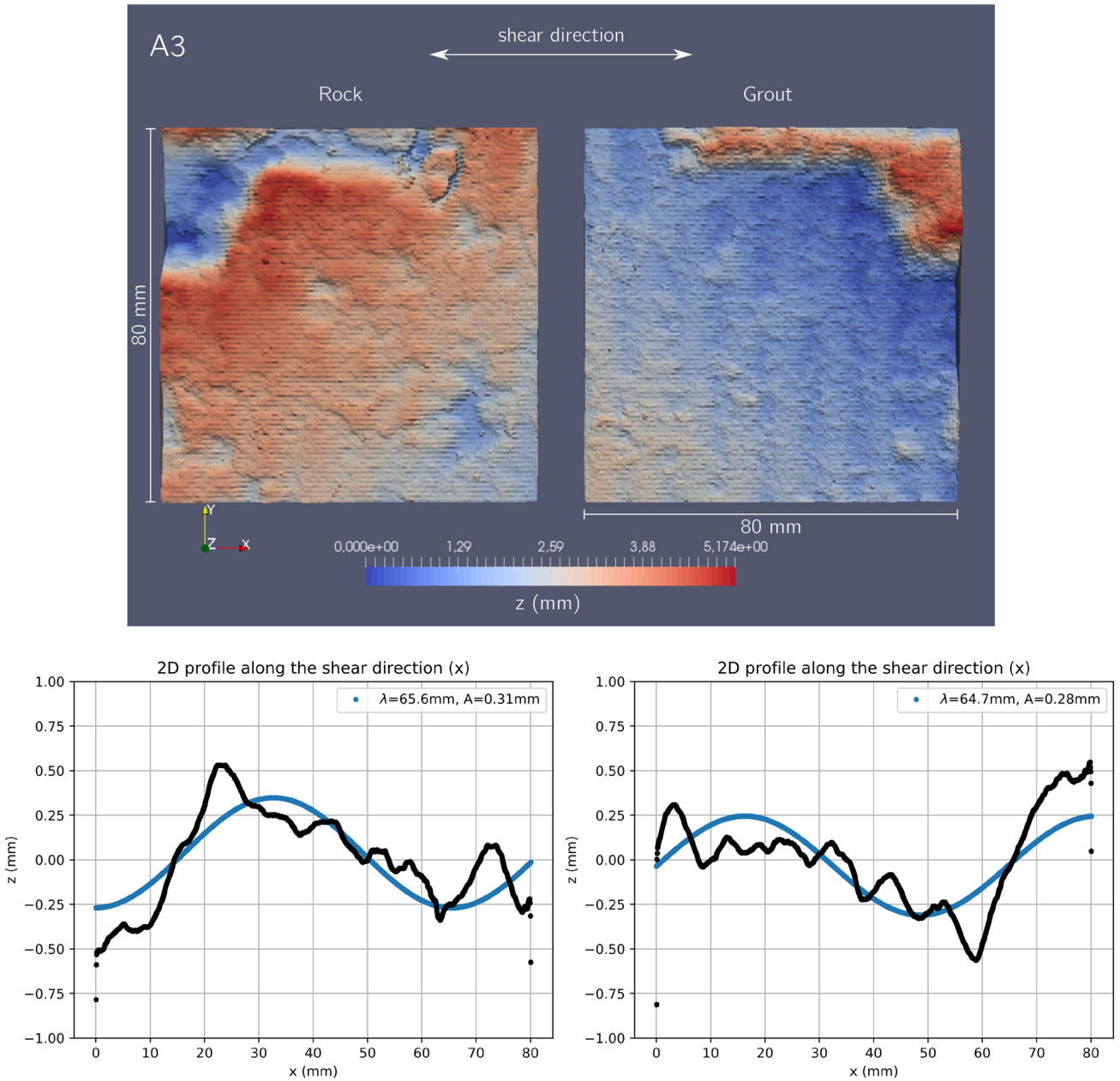

Fig. 25 Top: post shear scans of the rock/grout interface sample A3, bottom: average 2D-profiles along the shear direction (black) and fitted principal profile (blue); rock (left) and grout (right)

last being the most representative of the in situ conditions. Both unbonded rock/rock and bonded rock/grout interfaces of a given regular triangular roughness are tested under wet conditions. The shear response is as expected higher for the bonded rock/grout interface and it presents a more variable response. The post-shear state of all bonded rock/grout interfaces has resulted in a limestone layer of variable roughness attached on the grout surface. This is not the case when there is no pre-existing adhesion between the two materials composing the interface; under the given level of normal stress, the initial triangular roughness is traceable—and in the case of the grout well preserved—in the post-shear state of an unbonded prefabricated grout/rock interface and accurately depicted in the mechanical response (dilatancy and compaction corresponding to the asperity inclination).

The characterisation of the interface under monotonic loading has contributed to the design of a following experimental campaign with shear tests on the rough rock/grout interface under cyclic loading. All cyclic tests are performed under CNS and in wet conditions with an applied loading (average and cyclic) that is a function of the previously calculated shear strength. Two-way cyclic tests reach failure

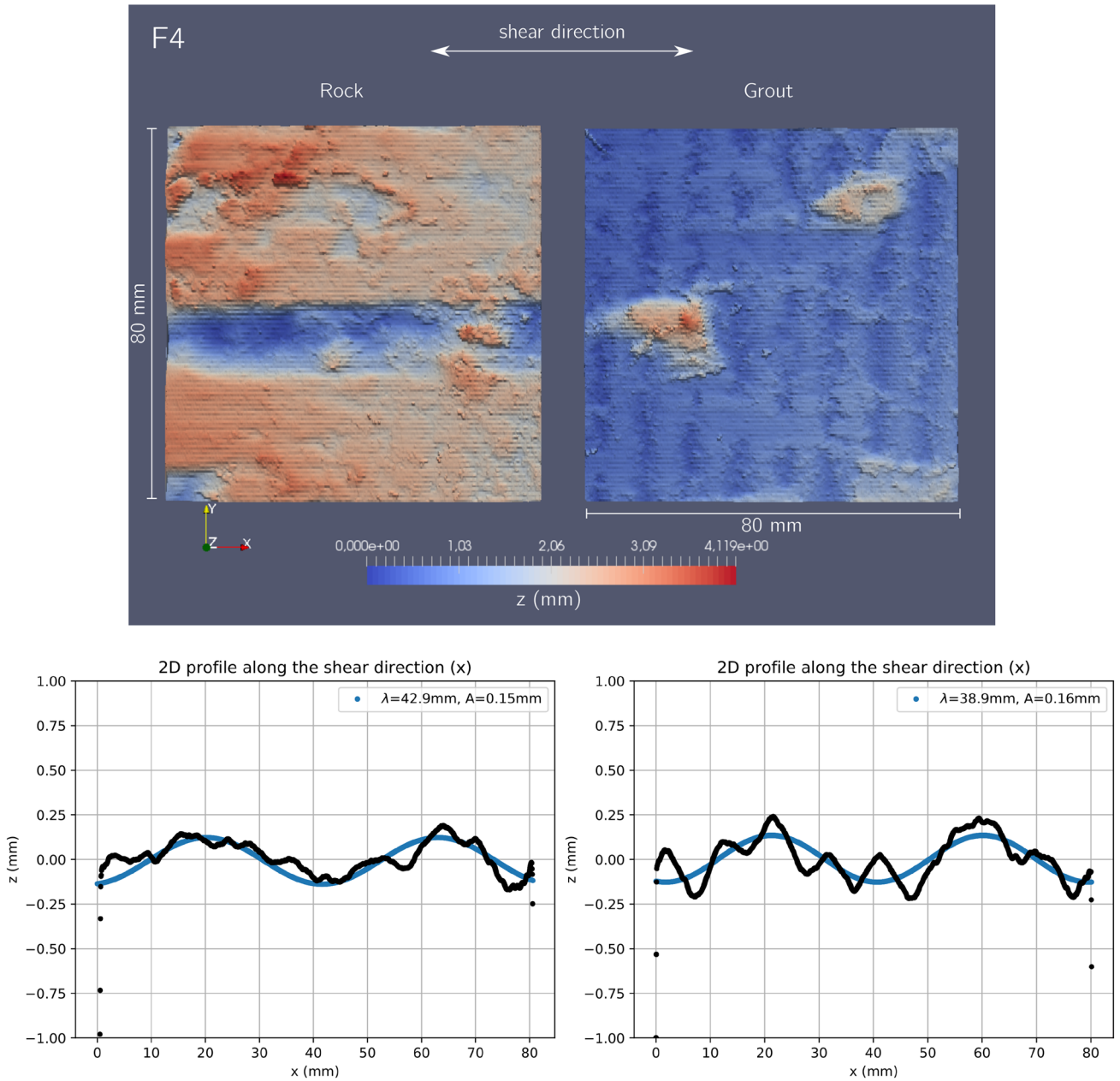

Fig. 26 Top: post shear scans of the rock/grout interface sample F4, bottom: average 2D-profiles along the shear direction (black) and fitted principal profile (blue); rock (left) and grout (right)

sooner comparing to one-way, the last being less damaging. A significant variability in the failure mode of the interface is observed among the different samples, even when tested under the same loading conditions. The heterogeneous nature of the limestone together with its interaction with the cast grout, leads to cracking in the limestone already after the application of the normal stress. The non-predictable creation of cracks of variable orientation, adds to the variable response of the given interface. During the cycles, the shear response of the interface involves progressively, with progressive evolution of its geometrical and mechanical state. Very interestingly, this variability in shear response seems to disappear after failure, with a final rock/grout interface exhibiting a similar residual response.

The occurring failure surface seems to pilot the mechanical response of the rock/grout interface with the alteration of the initial roughness and the creation of bigger asperities that dominate the response. This geometrical influence of the interfacial zone to the overall response should be studied in the future taking into account the scale effect and testing

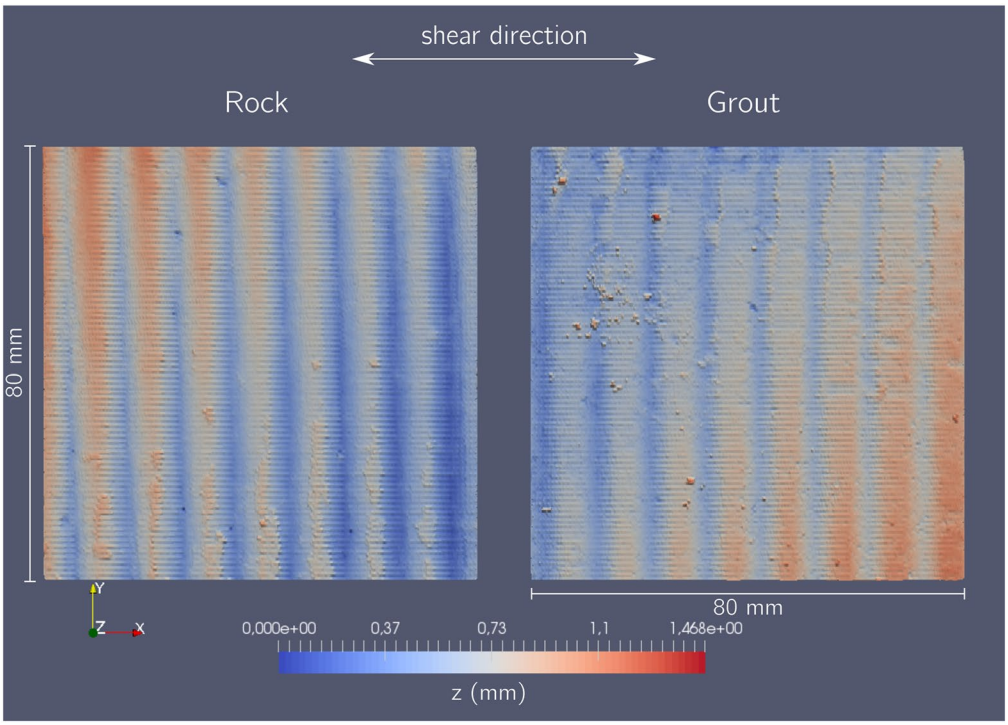

Fig. 27 Post shear scans of the prefabricated grout/rock interface

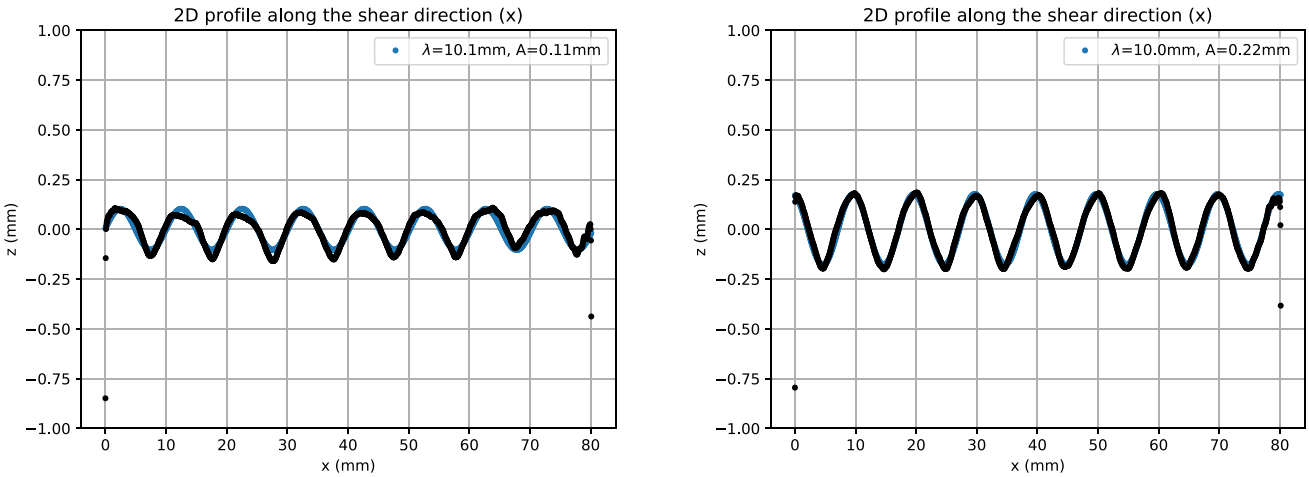

Fig. 28 Average 2D-profiles along the shear direction (black) and fitted principal profile (blue), left: rock and right: prefabricated grout

samples of different size. The rock/grout interaction modifies the initial roughness of a regular sawtooth and this influence would be interesting to be examined considering a different asperities size.

Finally, the post-shear morphological state of the tested interface samples has been illustrated. The two surfaces composing each sample are scanned after the end of the shear test and their topological maps are plotted allowing further observation of the geometrical evolution of the interface after failure. The average 2D profile of each surface is calculated, on which a profile based on the principal frequency of the Fourier transform is fitted, in an aim to characterise the roughness of the surface. The level of damage can only be observed in a qualitative way based on the overall 2D fitted profile compared to the initial roughness. In the case of the rock/grout interfaces, the initial roughness is not easily observed in the post-shear state, in particular on the limestone surface. The two surfaces, which in principle are

quite complementary, present an irregular profile resulting from the failure of limestone. In the case of two-way symmetric loading the created large asperities are found in the center of the rectangular surface, unlike the non-symmetric or one-way cyclic loading where the created asperities are observed closer to the edge. In either cases the creation of wet gouge during the shearing seems to contribute to the alternation of the final shape of the limestone surface.

All in all, in weak carbonate rock interfaces where the properties of the grout are extremely higher, the behaviour of the interface is governed by the that of the rock and thus, their study through CNS testing does not directly contribute in the improvement of the monopiles design. However, this should not be the case for stronger rocks with properties similar to the in-contact grout, where the interface is expected to dominate the response. In the presence of roughness, the expected geometrical dilation (limited elimination of the existing asperities) leads to the increase of the interface's normal stress and consequently, the apparent shear resistance is also expected higher. In this second case, CNS testing is supposed to provide important insight for the optimisation of the piles design.

A more quantitative analysis of the post-shear surfaces, could give a better idea for the characterisation of the interface's damage, both compared between the different tests and between the two parts of the surface itself. However, the prediction of the shape of the failure surface most probably requires the a priori knowledge of the microstructure of the limestone sample, the heterogeneity of which can result to completely different responses. Finally, the influence of the level of applied loads and the boundary conditions, as well as the scale effect should be considered for the stability of pile foundations.

Acknowledgements This work benefited from France Energies Marines and French National Research Agency (Investements for the Future) funds SOLCYP+: ANR-10-IEED-0006-18. The Authors wish also to thank Fawzi Karmous (Laboratoire 3SR) for the preparation of the rock samples.

Funding Open Access funding provided by EPFL Lausanne.

Compliance with Ethical Standards

Conflicts of interest The authors declare that they have no conflict of interest.

References

Alonso EE, Tapias M, Gili J (2012) Scale effects in rockfill behaviour. Géotech Lett 2(3):155–160

Assefa S, McCann C, Sothcott J (2003) Velocities of compressional and shear waves in limestones. Geophys Prospect 51(1):1–13

Baechle GT, Weger RJ, Eberli GP, Massaferro JL, Sun YF (2005) Changes of shear moduli in carbonate rocks: implications for Gassmann applicability. Lead Edge 24(5):507–510

Barton N, Choubey V (1977) The shear strength of rock joints in theory and practice. Rock Mech 10(1–2):1–54

Boulon M (1995) A 3-D direct shear device for testing the mechanical behaviour and the hydraulic conductivity of rock joints. In: Proceedings of mechanics of jointed and faulted rock

Boulon M, Plytas C, Foray P (1986) Comportement d'interface et prévision du frottement latéral le long des pieux et tirants d'ancrage. Revue française de géotechnique 35:31–48

Det Norske Veritas AS (2013) Offshore Standard DNV-OS-C502. Offshore Concrete Structures, September

Di Prisco CG, Muir Wood D (2012) Mechanical behaviour of soils under environmentally-induced cyclic loads, vol 534. Springer, Berlin

Heuze FE (1979) Dilatant effects of rock joints. In: 4th ISRM congress. International Society for Rock Mechanics and Rock Engineering

Hutson RW, Dowding CH (1990) Joint asperity degradation during cyclic shear. Int J Rock Mech Min Sci Geomech Abstr 27(2)

Indraratna B (2010) Effect of soil-infilled joints on the stability of rock wedges formed in a tunnel roof. Int J Rock Mech Min Sci 47(5):739–751

Indraratna B, Welideniya H, Brown E (2005) A shear strength model for idealised infilled joints under constant normal stiffness. Géotechnique 55(3):215–26

Jardine RJ, Standing JR (2012) Field axial cyclic loading experiments on piles driven in sand. Soils Found 52(4):723–736

Johnston IW, Lam TS (1989) Shear behavior of regular triangular concrete/rock joints-analysis. J Geotech Eng 115(5):711–727

Johnston IW, Lam TSK, Williams AF (1987) Constant normal stiffness direct shear testing for socketed pile design in weak rock. Geotechnique 37(1):83–89

Ladanyi B, Archambault G (1969) Simulation of shear behavior of a jointed rock mass. In: The 11th US symposium on rock mechanics (USRMS). American Rock Mechanics Association

Lebedev M, Wilson ME, Mikhaltsevitch V (2014) An experimental study of solid matrix weakening in water-saturated Savonniéres limestone. Geophys Prospect 62(6):1253–1265

Leichnitz W (1985) Mechanical properties of rock joints. Int J Rock Mech Min Sci Geomech Abstr 22(5)

Liu JW, Cui L, Zhu N, Han B, Liu J (2019) Investigation of cyclic pile-sand interface weakening mechanism based on large-scale CNS cyclic direct shear tests. Ocean Eng 194:106650

Lotsberg I, Serednicki A, Oerlemans R, Bertnes H, Lervik A (2013) Capacity of cylindrical shaped grouted connections with shear keys in offshore structures. Struct Eng 91(1):42–48

Misaghi A, Negahban S, Landrø M, Javaherian A (2010) A comparison of rock physics models for fluid substitution in carbonate rocks. Explor Geophys 41(2):146–154

Nam MS (2004) Improved design for drilled shafts in rock. University of Houston, Houston

Nam MS, Vipulanandan S (2008) Roughness and unit side resistances of drilled shafts socketed in clay shale and limestone. J Geotech Geoenviron Eng 134(9):1272–1279

Patton FD (1966) Multiple modes of shear failure in rock. In: 1st ISRM congress. International Society for Rock Mechanics and Rock Engineering

Rhett DW, Lord CJ (2001) Water weakening in sedimentary rocks. In: DC Rocks 2001, the 38th US symposium on rock mechanics (USRMS). American Rock Mechanics Association

Røgen B, Fabricius IL, Japsen P, Høier C, Mavko G, Pedersen JM (2005) Ultrasonic velocities of North Sea chalk samples: influence of porosity, fluid content and texture. Geophys Prospect 53(4):481–496

Rossebø ØH, Brevik I, Ahmadi GR, Adam L (2005) Modeling of acoustic properties in carbonate rocks. In: SEG technical program expanded abstracts 2005. Society of Exploration Geophysicists, pp 1505–1508

Rozenbaum O, du Roscoat SR (2014) Representative elementary volume assessment of three-dimensional X-ray microtomography images of heterogeneous materials: Application to limestones. Phys Rev E 89(5):053304

Schaumann P, Bechtel A, Lochte-Holtgreven S (2010) Fatigue design for prevailing axially loaded grouted connections of offshore wind turbine support structures in deeper waters. In: Proceedings of the European wind energy conference, pp 2047–2054

Seidel JP, Collingwood B (2001) A new socket roughness factor for prediction of rock socket shaft resistance. Can Geotech J 38(1):138–153

Seidel JP, Haberfield CM (1995) Towards an understanding of joint roughness. Rock Mech Rock Eng 28(2):69–92

Seidel JP, Haberfield CM (2002) A theoretical model for rock joints subjected to constant normal stiffness direct shear. Int J Rock Mech Min Sci 39(5):539–553

Seidel JP, Haberfield CM (2002) Laboratory testing of concrete-rock joints in constant normal stiffness direct shear. Geotechn Test J 25(4):391–404

Stavropoulou E, Briffaut M, Dufour F, Camps G (2019) Time-dependent behaviour of the Callovo-Oxfordian claystone-concrete interface. J Rock Mech Geotech Eng

Tatone BSA, Grasselli G (2015) Characterization of the effect of normal load on the discontinuity morphology in direct shear specimens using X-ray micro-CT. Acta Geotechnica 10(1):31–54

Vanorio T, Mavko G (2011) Laboratory measurements of the acoustic and transport properties of carbonate rocks and their link with the amount of microcrystalline matrix. Geophysics 76(4):E105–E115